Electronic Supplementary Material (ESI) for Nanoscale Advances.
This journal is © The Royal Society of Chemistry 2024

Electronic Supplementary Information

1-Naphthylacetic Acid Appended Amino Acids-Based Hydrogel: Probing of the Supramolecular Catalysis of Ester Hydrolysis Reaction

Ruchika Bassan[a], Biplab Mondal[b], Mayank Varshney[c] and Subhasish Roy*[a]

[a] Department of chemistry Birla Institute of Technology and science-Pilani, K K Birla Goa Campus NH 17B, Zuarinagar, Sancoale, Goa 403726, India,

[b] School of Biological Sciences, Indian Association for the Cultivation of Science, 2A & 2B, Raja Subodh Chandra Mallick Rd, Jadavpur, Kolkata-700034, West Bengal

[c] Application Specialist, Characterization Division, Anton Paar India Pvt. Ltd. 582, Phase V, Udyog Vihar Industrial Area, Gurgaon – 122016 (Haryana), India.

E-mail: subhasishr@goa.bits-pilani.ac.in

Table of Content

	Topic Name	Page Number
1.	Experimental Section ……....	S5-S6
2.	Materials and methods ……	S6
3.	Instrumentations, Techniques and Discussion …….	S6
	3.1 Tgel measurements ……	S6
	3.2 UV-VIS spectroscopy ……..	S6
	3.3 X-Ray Diffraction …….....	S6
	3.4 FT-IR Spectroscopy ……	S6
	3.5 CD Spectroscopy …….....	S6
	3.6 FE-SEM ……..	S6
	3.7 Liquid Chromatography-Mass spectrometer ……..	S6
	3.8 NMR …….....	S6
	3.9 Zeta Potential ……	S6
	3.10 Catalytic Study ……	S6-S7
	3.11 Rheology …….....	S7
	3.12 Confocal Microscopy …….....	S7
	3.13 pH measurements …….....	S7
4.	Synthesis of ^{L}***Nap-F*** and ^{D}***Nap-F*** …….....	S7
	4.1 Synthesis of 1-Naphthaleneacetic acid-conjugated L-phenylalanine methyl ester (***Nap-F***-OMe) …….....	S7
	4.2 Synthesis of 1-Naphthaleneacetic acid-conjugated L-phenylalanine carboxylic acid (***Nap-F***-OH or ***Nap-F***) …….....	S8
	4.3 Synthesis of 1-Naphthaleneacetic acid-conjugated D-phenylalanine methyl ester (1-Nap-D-***Nap-F***-OMe) (***Nap-F***-OMe) …….....	S8
	4.4 Synthesis of 1-Naphthaleneacetic acid-conjugated D-phenylalanine carboxylic acid (1-Nap-D-***Nap-F***-OH) (***Nap-F***-OH or ***Nap-F***) …….....	S9
Figure S1.	LC-MS spectrum of ^{L}***Nap-F***-OMe …….....	S10
Figure S2.	LC-MS spectrum of ^{D}***Nap-F***-OMe. …….	S10
Figure S3.	500 MHz ^{1}H NMR spectrum of ^{L}***Nap-F***-OMe …….....	S11
Figure S4.	500 MHz ^{1}H NMR spectrum of ^{D}***Nap-F***-OMe …….....	S11
Figure S5.	125 MHz ^{13}C spectrum of ^{L}***Nap-F***-OMe ……	S12
Figure S6.	125 MHz 13C spectrum of ^{D}***Nap-F***-OMe …….....	S12
Figure S7.	125 MHz DEPT-135 NMR spectrum of ^{L}***Nap-F***-OMe …….....	S13
Figure S8.	125 MHz DEPT-135 NMR spectrum of ^{D}***Nap-F***-OMe …….	S13
Figure S9.	LC-MS spectra of ^{L}***Nap-F***-OH …….....	S14
Figure S10.	LC-MS spectra of ^{D}***Nap-F***-OH …….....	S14
Figure S11.	LC-MS spectra of ^{L}***Nap-F***-OH …….....	S15

Figure S12. 500 MHz ^{1}H NMR spectrum of ^{D}***Nap-F***-OH S15

Figure S13. 125 MHz ^{13}C spectrum of ^{L}***Nap-F***-OH S16

Figure S14. 125 MHz ^{13}C spectrum of ^{D}***Nap-F***-OH S16

Figure S15. 125 MHz DEPT-135 NMR spectrum of ^{L}***Nap-F***-OH S17

Figure S16. 125 MHz DEPT-135 NMR spectrum of ^{D}***Nap-F***-OH S17

Figure S17. T_{gel} profile of the native **N*ap*-F$_{H-K}$** and **N*ap*-F$_{H-R}$** hydrogels. Error bars are shown inside the symbol as standard deviation S18

Figure S18. UV-Vis spectroscopic studies of the for mono (**N*ap*-F**), two (**N*ap*-F$_{H}$**, **N*ap*-F$_{K}$** and **N*ap*-F$_{R}$**), three (**N*ap*-F$_{H-K}$**, **N*ap*-F$_{H-R}$** and **N*ap*-F$_{K-R}$**) and four component (**N*ap*-F$_{H-K-R}$*)* hydrogels and in their solutions states S18

Table S1. X-ray diffraction major and minor peaks present for all the xerogels of mono (**N*ap*-F**), two (**N*ap*-F$_{H}$**, **N*ap*-F$_{K}$** and **N*ap*-F$_{R}$**), three (**N*ap*-F$_{H-K}$**, **N*ap*-F$_{H-R}$** and **N*ap*-F$_{K-R}$**) and four component (**N*ap*-F$_{H-K-R}$*)* hydrogels in their assembled state S19

Figure S19. FT-IR spectra of **N*ap*-F** bulk, mono (**N*ap*-F**), two (**N*ap*-F$_{H}$**, **N*ap*-F$_{K}$** and **N*ap*-F$_{R}$*)***, three (**N*ap*-F$_{H-K}$**, **N*ap*-F$_{H-R}$** and **N*ap*-F$_{K-R}$**) and four components (**N*ap*-F$_{H-K-R}$*)*** xerogels in KBr..... S20

Figure S20. FTIR-ATR spectra of ***Nap-F*** bulk and two **N*ap*-F$_{H}$**, **N*ap*-F$_{K}$** and **N*ap*-F$_{R}$** hydrogels in D_2O S20

Figure S21. Circular Dichroism spectroscopic responses of the mono (**Nap-F**), two (**Nap-F$_{H}$, N*ap*-F$_{K}$ and Nap-F$_{R}$**), three (**Nap-F$_{H-K}$, Nap-F$_{H-R}$ and Nap-F$_{K-R}$**) and four-component (**Nap-F$_{H-K-R}$**) hydrogels at 0.8 % w/v concentrations and half diluted hydrogels for both L-and D-amino acids-based assembled systems S21

Figure S22. Responses of I_1/I_3 in the pyrene emission spectra as a function of the concentration of the native, two-, three- and four-component assembled systems. Pyrene concentration kept at 10^{-6} M in all the measurements S21

Figure S23. FE-SEM images at assembled solutions of **(a)** ^{D}**Nap-F$_{K}$** and **(b)** ^{D}**Nap-F$_{K-R}$** after 50 times dilution at 0.01 % w/v concentrations S22

Table S2. Handedness of the helical fibers S22

Figure S24. FE-SEM images at assembled solutions of **(a)** ^{D}**Nap-F$_{K}$** and **(b)** ^{D}**Nap-F$_{K-R}$** after 50 times dilution at 0.01 % w/v concentrations S22

Figure S25. TEM image of **Nap-F$_{K-R}$** showing helical twisted fibers. S23

Figure S26. Confocal microscopic images of the hydrogels at 0.8 w/v % concentrations **(a)** & **(b)** for **Nap-F**; **(c)** & **(d)** for **Nap-F$_{H}$** (6:2); **(e)** & **(f)** **Nap-F$_{K}$** (6:2)**; (g)** & **(h)** for **Nap-F$_{R}$** (6:2); **(i)** & **(j)** for **Nap-F$_{H-K}$** (6:1:1); **(k)** & **(l)** for **Nap-F$_{H-R}$** (6:1:1)**; (m)** & **(n)** **Nap-F$_{K-R}$** (6:1:1) and **(o)** & **(p)** for **Nap-F$_{H-K-R}$** (5:1:1:1) under bright field and dark field at **405 nm** respectively S23

Figure S27. Absorbance vs Concentration plot for determination of molar extinction coefficient (ε) of *p*- nitrophenol in water S24

Figure S28. The progress of the *p*-**NPA** to *p*-**NP** hydrolysis reaction monitored by time dependent UV-Vis spectroscopic study for the systems including a) **H-K**, (b) **H-R**, (c) **K-R**, (d) **Nap-F$_{K}$**, (e) **Nap-F$_{R}$**, (f) **Nap-F$_{H-K}$**, (g) **Nap-F$_{H-R}$**, (h) **Nap-F$_{K-R}$**, (i) **Nap-F$_{H-K-R}$** and (j) **NaOH** S24

Figure S29. Lineweaver-Bruk plot for the hydrolysis of *p*-**NPA** by using various systems as catalysts such as **H-K**, **H-R**, **K-R**, N**ap**-F$_{K}$, N**ap**-F$_{R}$, N**ap**-F$_{H-K}$, N**ap**-F$_{H-R}$, N**ap**-F$_{K-R}$, N**ap**-F$_{H-K-R}$ and **NaOH** S25

Table S3. Kinetic parameters for the hydrolysis of PNPA in the presence of catalysts system. The Michaelis–Menten kinetics equation $v = \frac{d[P]}{dt} = \frac{K_{cat}}{K_m}[E]_0[S]$ and double-reciprocal (Lineweaver–Burk) method with the equation $v = \frac{d[P]}{dt} = K_{cat}[E]_0\frac{[S]}{K_M + [S]}$ were used where v is reaction rate, [P] is concentration of product, $[E]_0$ is the initial enzyme concentration, [S] is substrate (p-nitrophenyl acetate) concentration, k_{cat} is the catalytic rate constant, and K_M is the Michaelis constant. The k_{cat}/K_M values calculated from the linear fitting of the double-reciprocal (Lineweaver–Burk) plot (Figure S29) S25

Figure S30. FE-SEM of **(a)** **Nap-F$_{K}$** and **(b)** **Nap-F$_{K-R}$** after the catalysis suggesting the stability of the co-assembles structures S26

Figure S31. ESI-MS of the catalytic mixture solution by **Nap-F$_{K-R}$** showing the corresponding molecular ion peak for *p*-nitrophenolate at m/z 138 and with one sodium ion at m/z 160.80. The peak at m/z 99.70 is originating may be form the acetic acid with one potassium ion S26

Table S4. pHs of the assembled systems before and after the p-PNPA hydrolysis ……. S26

Table S5. LC-ESI-MS analyses of the mass peaks obtained shown in Figure S31-41 in positive mode at lower voltages including 50 and 70 V ……. S27-28

Figure S32-Figure 42 LC-ESI-MS analyses of all the catalytic systems ……. S28-S33

Figure S43. Lineweaver-Bruk plot for the hydrolysis of PNPA using **Nap-F$_{K-R}$** as catalyst keeping the amount of **K** and **R** fixed, the amount of **Nap-F** varied **(a) Nap-F** at 0.1 w/v%, **(b) Nap-F** at 0.2 w/v% and **(d) Nap-F** at 0.3 w/v% for the system 0.3 % w/v, 0.4 % w/v and 0.5 % w/v catalysts respectively ……..... S34

Figure S44. UV-Vis spectra for the hydrolysis of PNPA using **Nap-F$_{K-R}$** as catalyst keeping the amount of **K** and **R** fixed, the amount of **Nap-F** varied **(a) Nap-F** at 0.1 w/v%, **(b) Nap-F** at 0.2 w/v% and **(d) Nap-F** at 0.3 w/v% for the system 0.3 % w/v, 0.4 % w/v and 0.5 % w/v catalysts respectively …… S34

Figure S45. Absorbance vs Concentration plot for determination of molar extinction coefficient (ε) of p- nitrophenol at pH 9.00. S35

Figure S46. The progress of the *p*-**NPA** to *p*-**NP** hydrolysis reaction monitored at pH 9.00 by time dependent UV-Vis spectroscopic study for the systems including a) **H-K**, (b) **H-R**, (c) **K-R**, (d) **H-K-R**, (e) **Nap-F$_H$**, (f) **Nap-F$_K$**, (g) **Nap-F$_R$**, (h) **Nap-F$_{H-K}$**, (i) **Nap-F$_{H-R}$**, (k) **Nap-F$_{K-R}$**, and (l) **Nap-F$_{H-K-R}$**. S35

Figure S47. Lineweaver-Bruk plot for the hydrolysis of p-NPA by using various systems as catalysts at pH 9.00 such as **Nap-F$_H$**, **Nap-F$_K$**, **Nap-F$_R$**, **Nap-F$_{H-K}$**, **Nap-F$_{H-R}$**, **Nap-F$_{K-R}$** and **Nap-F$_{H-K-R}$**. S36

Figure S48. Absorbance versus time spectra for **Nap-F$_H$**, **Nap-F$_K$**, **Nap-F$_R$**, **Nap-F$_{H-K}$**, **Nap-F$_{H-R}$**, **Nap-F$_{K-R}$**, **Nap-F$_{H-K-R}$**, **H-R**, **H-K**, **K-R** and **H-K-R** at 0.5% w/v concentrations of pH 9.00 with 3µl working solution of *p*-**NPA** . S36

Table S6. Kinetic parameters for the hydrolysis of PNPA in the presence of catalysts system at pH 9.00. The Michaelis–Menten kinetics equation v = $\frac{d[P]}{dt} = \frac{K_{cat}}{K_m}[E]_0[S]$ and double-reciprocal (Lineweaver–Burk) method with the equation v = $\frac{d[P]}{dt} = K_{cat}[E]_0\frac{[S]}{K_M + [S]}$ were used where v is reaction rate, [P] is concentration of product, $[E]_0$ is the initial enzyme concentration, [S] is substrate (p-nitrophenyl acetate) concentration, k_{cat} is the catalytic rate constant, and K_M is the Michaelis constant. The k_{cat}/K_M values calculated from the linear fitting of the double-reciprocal (Lineweaver–Burk) plot (Figure S47) S37

Figure S49. FE-SEM images at assembled solutions of pH 9.00 (50 times dilution for all samples done from 0.5 w/v % co-assembled solution) which have been used for catalytic studies (a) **NAP-F$_K$** 2.5:2.5, (b) **NAP-F$_{H-K}$** 3:1:1 and (c) **NAP-F$_{K-R}$** 3:1:1 (0.5 w/v %). S37

1. Experimental Section:

All the chemicals purchased from various suppliers were used without further purification. The L-phenylalanine derivative of 1-Naphthaleneacetic acid (**Nap-F** ester) was synthesized following conventional solution phase peptide synthetic protocols by coupling methyl ester of L-phenylalanine and 1-Naphthaleneacetic acid by using HoBt and DCC as coupling agent. The purification of the **Nap-F** ester was carried out by using petroleum ether with an increasing amount of ethyl acetate. The methyl ester of the **Nap-F** was hydrolyzed following the saponification of the ester method. The free carboxylic acid of the **Nap-F** was used for further studies. The details of synthetic protocols, purifications and their characterizations by using NMR and mass spectrometric analyses were shown in Figure S1 to Figure S16. The hydrogelation behaviour of both ^{L} **Nap-F** and ^{D} **Nap-F** and their co-assembled hydrogels were quite similar.

1.1 Two-component gelation

Nap-F along with either of the three basic amino acids L-Histidine (**H**), L-Lysine (**K**) and L-Arginine (**R**) separately were taken together in a single glass vial and the gelation study was performed as follows: i) in one vial **Nap-F** and **H** were mixed (**Nap-F$_{H}$**), (ii) in second vial **Nap-F** and **K** were mixed (**Nap-F$_{K}$**) and (iii) in third glass vial **F** and **R** were mixed (**Nap-F$_{R}$**) in different ratios to check the gelation of these samples. These suspended solutions were sonicated and heated on a hot plate until a clear solution was obtained. These hot clear solutions were kept at room atmosphere undisturbed for 5 to 10 minutes and hydrogelations were confirmed by inverted vial test method. Moreover, individually **Nap-F** does not form a hydrogel in distilled water (DW) however, in the presence of either of these basic amino acids, **Nap-F** formed two-component stable hydrogels in water (Figure 1b, 1c and 1d, Table 1).

1.2 Three-component gelation

Nap-F in combination with either of the two basic amino acids were taken and the gelation study were performed as follows: i) in one vial **Nap-F**, **H** and **K** were mixed (**Nap-F$_{H-K}$**), (ii) in second vial **F**, **H and R** were mixed (**Nap-F$_{H-R}$**) and (iii) in the third glass vial **F, K** and **R** were mixed (**Nap-F$_{K-R}$**) in different ratios to check the gelation of these samples. These suspended solutions were sonicated followed by heating on a hot plate until clear solutions were obtained. These hot clear solutions were kept at room atmosphere and hydrogelations were confirmed by an inverted vial test method. It was observed that individually **Nap-F** not formed hydrogel in distilled water (DW) however, in combination with either of the two basic amino acids, **Nap-F** formed three-component stable hydrogels in water (Figure 1e, 1f and 1g, Table 1).

1.3 Four-component gelation

Nap-F along with all three basic amino acids L-Histidine (**H**), L-Lysine (**K**) and L-Arginine (**R**) were taken together in a single glass vial and the gelation study have been performed. These suspended solutions (**Nap-F$_{H-K-R}$**) were sonicated and heated on a hot plate until clear solutions were obtained. On keeping this four-component hot solution in room atmosphere undisturbed for 5 to 10 minutes, hydrogelation was observed and confirmed by the inverted vial method. This hydrogel is also obtained in water (Figure 1h, Table 1).

The minimum gelation concentrations (MGCs) of all these hydrogels have been estimated and shown in Table 1. **Nap-F_K** at a 6:2 weight ratio forms hydrogel with MGC of 0.21 % w/v which is the lowest MGC among all these hydrogels and **NAP-F** shows the highest MGC of 0.7 % w/v. **Nap-F_H** also shows a similar MGC value of 0.22 % w/v.

1.4 Xerogel preparation

All the xerogels were prepared by freeze drying the hydrogels in the Lyophilizer and used for various experiments in powder forms.

2. Materials and methods

1-Naphthaleneacetic acid was purchased from Sigma Aldrich. L-Phenylalanine, DCC (N, N'-dicyclohexylcarbodiimide) was purchased from Molychem. HOBt (1-hydroxybenzotriazole) was purchased from Spectrochem. *p*-nitrophenyl acetate (PNP) was purchased from TCI.

3. Instrumentations, Techniques and Discussion:

3.1 Tgel measurement: Different (0.7, 0.75, 0.8, 0.85, 0.9, 0.95, 1.0) % w/v hydrogels of **Nap-F** were prepared by dissolving in phosphate buffer (PB, 50mM) of pH-7.4. All these two, three and four component hydrogelators at
0.8 % w/v concentrations were dissolved in milli Q water, by using sonication followed by heating the solution, until it dissolves completely. At three different concentrations keeping the ratio 6 : 1 : 1 for **Nap-F_{H-K}** and **Nap-F_{H-R}** and Tgels were measured. The solutions were kept at rest until it comes to room temperature. The hydrogelations of the samples were confirmed by the vial inversion test method. All these gels at 0.8 % w/v were heated in a water bath to check their melting points (Tgel, temperature at which the hydrogels were melted).

3.2 UV-Vis spectroscopy: UV-Visible spectra were recorded by using a JASCO V-550, and the bandwidth and data pitch was set at 1 nm.

3.3 X-Ray Diffraction: The xerogels were characterized by X-ray diffraction (XRD) by using a powder X-ray diffractometer (Bruker D8 Advance) with Cu-Kα (λ=0.154 nm).

3.4 FT-IR Spectroscopy: IR Affinity-1 (Shimadzu, Japan) FTIR spectrophotometer was used to record IR spectra and KBr was used to prepare pellets before recording IR spectra.

3.5 CD Spectroscopic Study. The circular dichroism (CD) spectroscopic study was recorded on a JASCO J-810 circular dichroism spectrometer at room temperature. Spectra were scanned at a scan rate of 200 nm/s and 2 nm bandwidth from 190 to 500 nm and the average profile of three different scans were shown in the spectra. Baseline corrections with sample media were performed before the experiments.

3.6 FE-SEM: The gelator solutions (0.25 micromolar) were dropped cast on a glass cover slip. Leica EM ACE200 was used to coat the sample with the gold at a few nm thicknesses. The images were taken under an FEI Quanta FEG 250 scanning electron microscope.

3.7 TEM: TEM imaging were carried out by using a JEOL JEM-210 PLUSCryogenic transmission electron microscope.

3.8 Liquid Chromatography-Mass spectrometry: This data was obtained from Agilent triple quad LCMS 6460 to determine the molecular mass of compounds in the electrospray ionization (ESI +/-) mode.

3.9 NMR: These spectra were recorded on Bruker Avance Neo 500 MHz with Cryoprobe plateform, Topspin controlled console and gradient control with a resolution of 12.5 ns. $CDCl_3$ and DMSO-d_6 were the solvents used.

3.10 Zeta Potential: Zeta potential measurements were performed by using NanoPlus-Zeta/nano particle analyzer particulate system in water.

3.11 Catalytic Study: The molar extinction coefficient (ε) of *p*-nitrophenol (PNP) was estimated in water from

the slope of the linear plot between absorption maxima at 400 nm versus concentrations of the *p*-nitrophenol 3 µL of 3 mM *p*-nitrophenyl acetate has been added individually to all these assembled systems and the progress of hydrolysis have been monitored by UV-vis spectroscopy. The Michaelis–Menten kinetics equation v = $\frac{d[P]}{dt} = \frac{K_{cat}}{K_m}[E]_0[S]$ and double-reciprocal (Lineweaver–Burk) method with the equation v = $\frac{d[P]}{dt} = K_{cat}[E]_0\frac{[S]}{K_M + [S]}$ were used where v is reaction rate, [P] is concentration of product, $[E]_0$ is the initial enzyme concentration, [S] is substrate (p-nitrophenyl acetate) concentration, k_{cat} is the catalytic rate constant, and K_M is the Michaelis constant. The k_{cat}/K_M values calculated from the linear fitting of the double-reciprocal (Lineweaver–Burk) plot.

3.12 Rheology: This measurement was done on Anton Paar, MCR 702e Space with a minimum torque limit of 0.5 nNm under oscillation mode and 1 nNm in rotation mode. The maximum torque limit was 230 mNm. Temperature control was performed by using P-PTD 200 and PP25/SP measuring geometry. The low shear condition was done at a strain of 0.1% and 10 rad/sec angular frequency, and the high shear condition was done at 100% strain and 10 rad/sec angular frequency. All the rheological studies of the hydrogels were performed after a week later from the date of hydrogel preparation.

3.13 Confocal Microscopy: All the hydrogelators solutions (0.5 % w/v) were dropped casted on glass slides. The self-assembled and co-assembled solutions were covered with cover slips for the confocal microscopy imaging purpose in their wet gel states. An Olympus corporation FV3000 model IX83 confocal laser scanning microscope (CLSM) was used for image capturing. A 405 nm laser diode was used as the excitation source and emission was recorded from 413–484 nm range was detected. The detector gain and amplification offset/gain were optimized based on the fluorescence intensities of the hydrogel fibrils.

3.14 pH measurements: The pHs of the catalytic solutions were measured by using THERMO SCIENTIFIC™ EUTECH™ pH meter and the calibration of the pH meter was performed by using standard pH solutions of pHs of 4, 7 and 9. The calibration error during the experiments were found to be ±0.36.

4. Synthesis of ^{L}**Nap-F** and ^{D}**Nap-F**

4.1 Synthesis of 1-Naphthaleneacetic acid-conjugated L-phenylalanine (Nap-*F-OMe or Nap-F-OMe*): L-phenylalanine (1.65g) was dissolved in methanol (25ml) in a round bottom flask (RBF) covered with a $CaCl_2$ glass guard tube. The solution was stirred inside a fume hood and kept for cooling by using ice-salt mixture bath. Once the solution was cooled down, 3-5 ml of $SOCl_2$ was added from the walls of the RBF and covered again with a guard tube and kept for overnight under constant stirring. The completion of the reaction has been confirmed by *TLC* and the methanol was distilled out until 5 ml remained followed by the addition of di-ethyl ether to the RBF and yellowish-white solid appeared inside the RBF. For extraction purposes, ethyl acetate was added and washing with Na_2CO_3 was performed. The ethyl acetate extract was dried over anhydrous Na_2SO_4 and evaporated in a vacuum to obtain 2-3 ml ethyl acetate solution of the phenylalanine methyl ester.

Now, 1-Naphthalenacetic acid (3.72g) was dissolved in dry N, N-dimethyl formamide (DMF) and kept under stirring condition to cool in an ice-salt bath. Once the solution cooled down, HOBt (1.53g) and DCC (3.09g) were added and stirred well. The final step included the addition of the ethyl acetate solution of the amino acid and kept for stirring for 2 days. The reaction mixture was diluted with ethyl acetate the filtered out to separate N, N-dicyclohexyl urea (DCU). The ethyl acetate layer was washed with 1N HCl, brine, and saturated Na_2CO_3 solution. The organic layer was then further dried over anhydrous Na_2SO_4, to obtain a yellowish product.

This product was further purified through by using silica gel column chromatography, to obtain a pure white product, which is the amino acid derivative (1-Nap-^{L}***F***-OMe) (***Nap-F***-OMe) The synthesis was confirmed by

performing LC-MS and NMR spectroscopic studies.

Yield: 49 %

LC-MS-ESI (+) (Figure S1): Observed peak corresponding to $M+1]^+$: at m/z 348.4, exact mass**:** 347.15

NMR (Figure S3, S5 and S7):

^{1}H NMR (500 MHz, $CDCl_3$) (Figure S3): δ 8.00 – 7.89 (ddd, *J* = 20.1, 6.2, 3.6 Hz, 2H), 7.88 – 7.83 (d, *J* = 8.3 Hz, 1H), 7.61 – 7.51 (dd, *J* = 6.4, 3.3 Hz, 2H), 7.48 – 7.41 (m, 1H), 7.39 – 7.34 (d, *J* = 6.9 Hz, 1H), 7.13 – 7.06 (m, 1H), 7.05 – 6.96 (t, *J* = 7.6 Hz, 2H), 6.61 – 6.54 (d, *J* = 7.8 Hz, 2H), 5.81 – 5.76 (d, *J* = 8.1 Hz, 1H), 4.91 – 4.83 (s, 1H), 3.67 – 3.63 (s, 3H), 2.91 – 2.91 (s, 2H).

^{13}C NMR (125 MHz, $CDCl_3$) (Figure S5): δ 171.56, 170.36, 135.26, 134.04, 132.05, 130.73, 128.85, 128.81, 128.52, 128.36, 128.34, 76.83, 52.78, 52.22, 41.61, 37.59, 33.98, 25.66, 24.98.

DEPT 135 (125 MHz, $CDCl_3$) (Figure S7): δ 129.04, 128.85, 128.81, 128.53, 128.44, 128.36, 128.34, 127.74, 126.87, 126.80, 126.22, 125.68, 123.84, 52.79, 52.22, 41.60, 37.57.

4.2 Synthesis of 1-Naphthaleneacetic acid-conjugated L-phenylalanine (Nap-*F-OH* *or* *Nap-F-OH* *or* *Nap-F* *in short*): Hydrolysis was performed by dissolving in methanol (10ml) and under the presence of 1N NaOH (5ml), the reaction was kept overnight. The progress of the reaction was confirmed by monitoring TLCs. Further, the methanol was evaporated and the aqueous part was washed with diethyl ether followed by acidification using 1N HCl. The aqueous layer was then extracted using ethyl acetate. The ethyl acetate extract was dried over anhydrous Na_2SO_4 and evaporated in a vacuum to obtain a white powdered product (1-Nap-^{L}F-OH) (***NAP-F***). The synthesis has been confirmed by performing LC-MS and NMR.

Yield: 85 %

LCMS-ESI (+) (Figure S9): Observed peak corresponding to $M+1]^+$: m/z 334.4 expected mass**:** 333.14

NMR (Figure S11, S13 and S15)

^{1}H NMR (500 MHz, DMSO-d_6) (Figure S11): δ 8.57 – 8.52 (d, *J* = 8.3 Hz, 1H), 7.97 – 7.92 (d, *J* = 8.3 Hz, 1H), 7.92 – 7.88 (d, *J* = 8.0 Hz, 1H), 7.82 – 7.77 (d, *J* = 8.1 Hz, 1H), 7.53 – 7.37 (m, 3H), 7.35 – 7.30 (d, *J* = 7.0 Hz, 1H), 7.30 – 7.19 (q, *J* = 7.3, 6.6 Hz, 5H), 4.52 – 4.44 (td, *J* = 9.5, 4.6 Hz, 1H), 3.97 – 3.87 (s, 1H), 3.14 – 3.07 (dd, *J* = 13.8, 4.6 Hz, 1H), 2.96 – 2.88 (dd, *J* = 13.8, 9.8 Hz, 1H).

^{13}C NMR (125 MHz, DMSO-d_6) (Figure S13): δ 173.57, 170.53, 138.09, 133.73, 133.02, 132.38, 129.61, 128.74, 128.64, 128.20, 127.46, 126.88, 126.35, 126.02, 125.88, 124.73, 54.02, 39.90, 37.26.

DEPT 135 (126 MHz, DMSO-d_6) (Figure S15): δ 132.37, 129.61, 128.74, 128.65, 128.20, 127.47, 126.88, 126.36, 126.02, 125.88, 124.72, 54.02, 39.81, 37.25.

The same protocol was used for the synthesis of 1-Naphthalenacetic acid appended D-phenylalanine and the corresponding characterizations results are as follows:

4.3 (1-Nap-^{D}F-OMe) (Nap**-F-OMe)**:

Yield: 57 %

LC-MS-ESI (+) (Figure S2): Observed peak corresponding to $[M]^+$: 347.70 exact mass**:** 347.15.

^{1}H NMR (500 MHz, $CDCl_3$) (Figure S4): δ 7.84 (ddd, J = 19.1, 6.3, 3.4 Hz, 2H), 7.75 (d, J = 8.2 Hz, 1H), 7.45 (dd, J = 6.3, 3.3 Hz, 2H), 7.34 (t, J = 7.6 Hz, 1H), 7.27 (s, 1H), 6.98 (d, J = 7.4 Hz, 1H), 6.88 (t, J = 7.6 Hz,

2H), 6.47 (d, J = 7.4 Hz, 2H), 5.67 (d, J = 8.1 Hz, 1H), 4.76 (dt, J = 8.0, 5.6 Hz, 1H), 3.99 (d, J = 16.3 Hz, 1H), 3.88 (d, J = 16.4 Hz, 1H), 3.54 (s, 3H), 1.11 – 0.96 (m, 1H).

^{13}C NMR (125 MHz, $CDCl_3$) (Figure S6): δ 171.65, 170.47, 135.33, 134.11, 132.15, 130.79, 128.94, 128.91, 128.62, 128.45, 126.96, 126.90, 126.32, 125.77, 123.93, 52.88, 52.32, 41.69, 37.66, 34.02, 25.73, 25.05.

DEPT 135 (125 MHz, $CDCl_3$) (Figure S8): δ 128.85, 128.81, 128.53, 128.36, 128.34, 126.87, 126.80, 126.22, 125.67, 123.83, 52.79, 52.22, 49.18, 41.60, 37.57, 33.93, 25.63, 24.95.

4.4 (1-Nap-*D*F-OMe) (Nap**-F-OH or N**ap**-F)**:

Yield: 85 %

LC-MS-ESI (+) (Figure S10): observed peak corresponding to $M]^+$ at m/z 333.70 exact mass**:** 333.14.

^{1}H NMR (500 MHz, DMSO-d_6) (Figure S12): δ 7.84 (ddd, J = 19.1, 6.3, 3.4 Hz, 2H), 7.75 (d, J = 8.2 Hz, 1H), 7.45 (dd, J = 6.3, 3.3 Hz, 2H), 7.34 (t, J = 7.6 Hz, 1H), 7.27 (s, 1H), 6.98 (d, J = 7.4 Hz, 1H), 6.88 (t, J = 7.6 Hz, 2H), 6.47 (d, J = 7.4 Hz, 2H), 5.67 (d, J = 8.1 Hz, 1H), 4.76 (dt, J = 8.0, 5.6 Hz, 1H), 3.99 (d, J = 16.3 Hz, 1H), 3.88 (d, J = 16.4 Hz, 1H), 3.54 (s, 3H), 1.11 – 0.96 (m, 1H).

^{13}C NMR (125 MHz, DMSO-d_6) (Figure S14): δ 173.10, 170.05, 137.63, 133.26, 129.14, 128.27, 128.17, 127.72, 126.99, 126.40, 125.89, 125.55, 125.41, 124.26, 53.57, 36.79.

DEPT 135 (125 MHz, DMSO-d_6) (Figure S16): δ 129.23, 128.36, 128.26, 127.81, 127.08, 126.49, 125.98, 125.64, 125.50, 124.35, 53.66, 36.88.

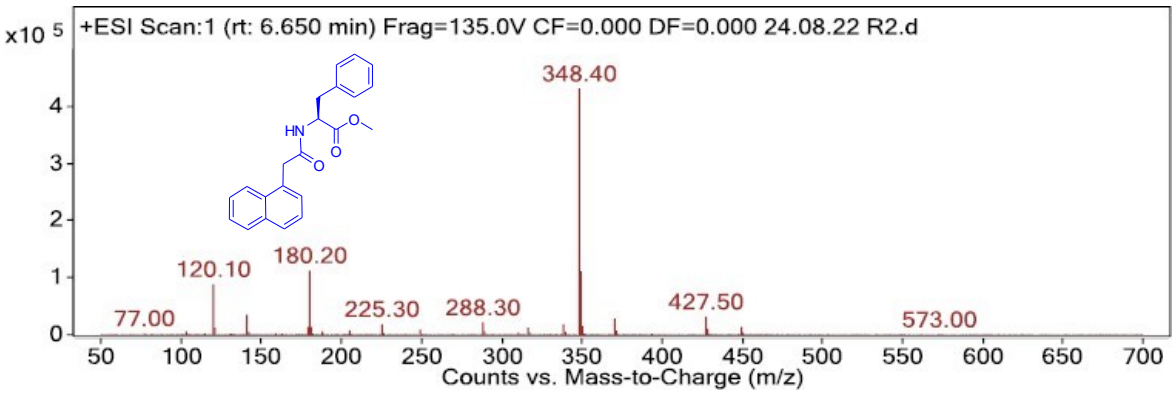

Figure S1. LC-MS spectrum of ^{L}***N*ap-*F*-OMe.

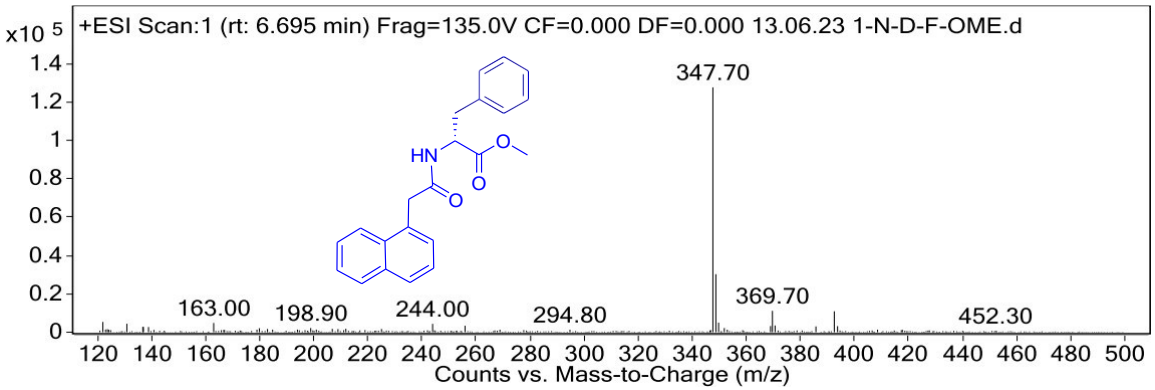

Figure S2. LC-MS spectrum of ^{D}***N*ap-*F*** -OMe.

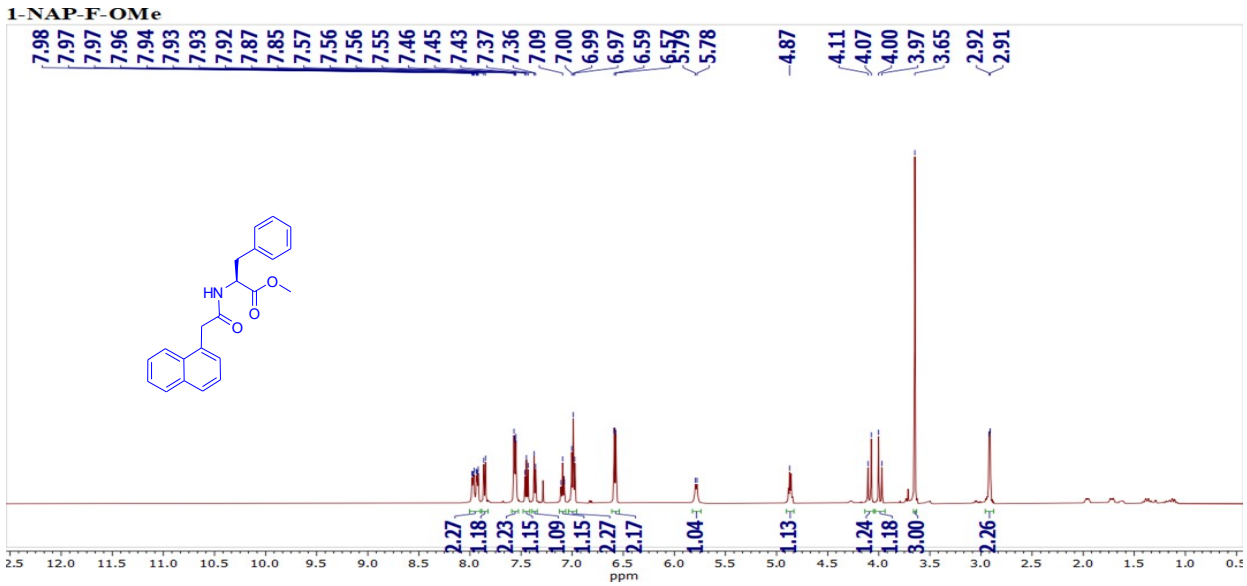

Figure S3. 500 MHz ^{1}H NMR spectrum of ^{L}***N*ap-*F*-OMe.

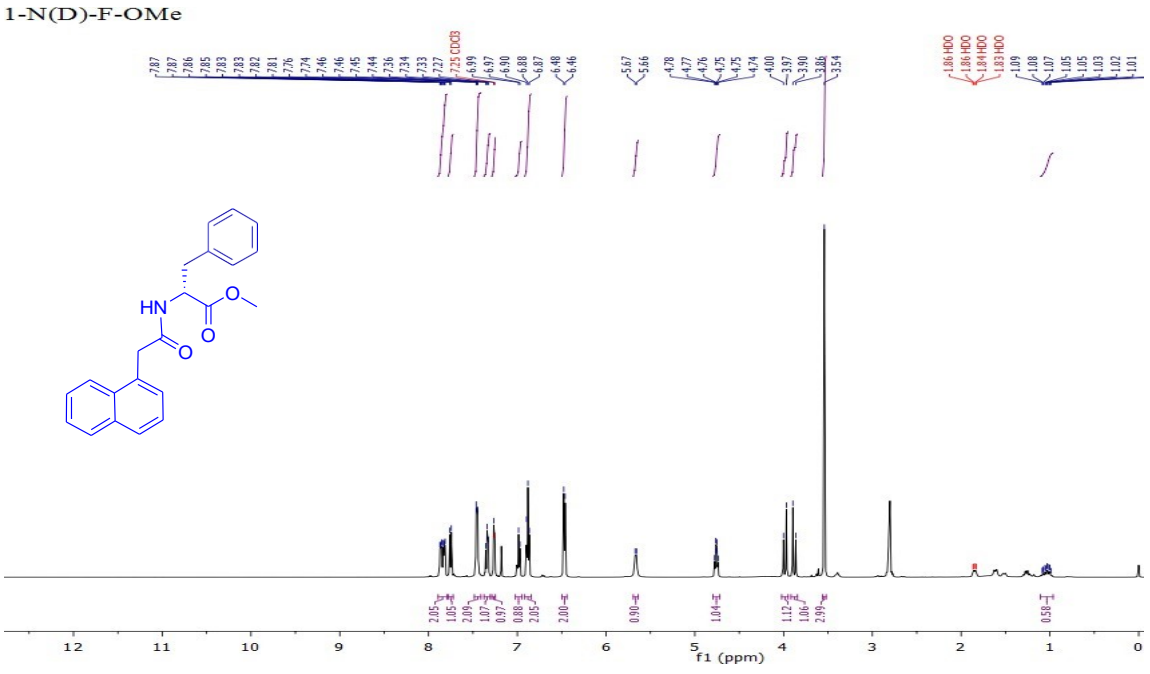

Figure S4. 500 MHz ^{1}H NMR spectrum of ^{D}***N*ap-*F*** -OMe.

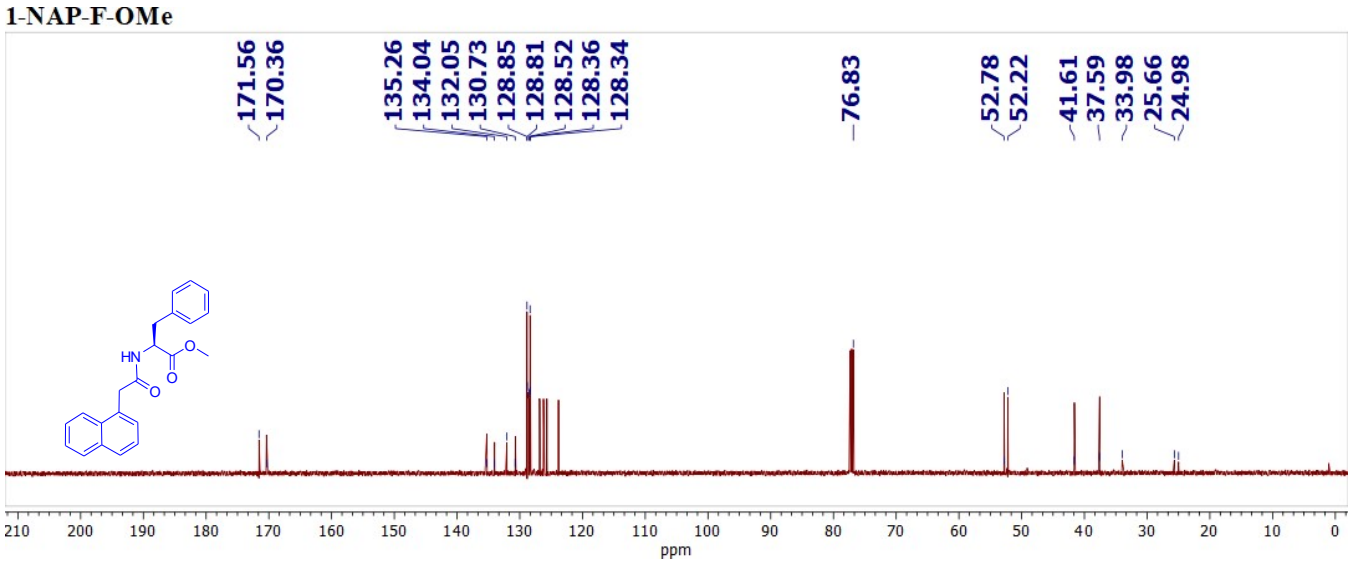

Figure S5. 125 MHz ^{13}C spectrum of ^{L}***N*ap-*F*-OMe.

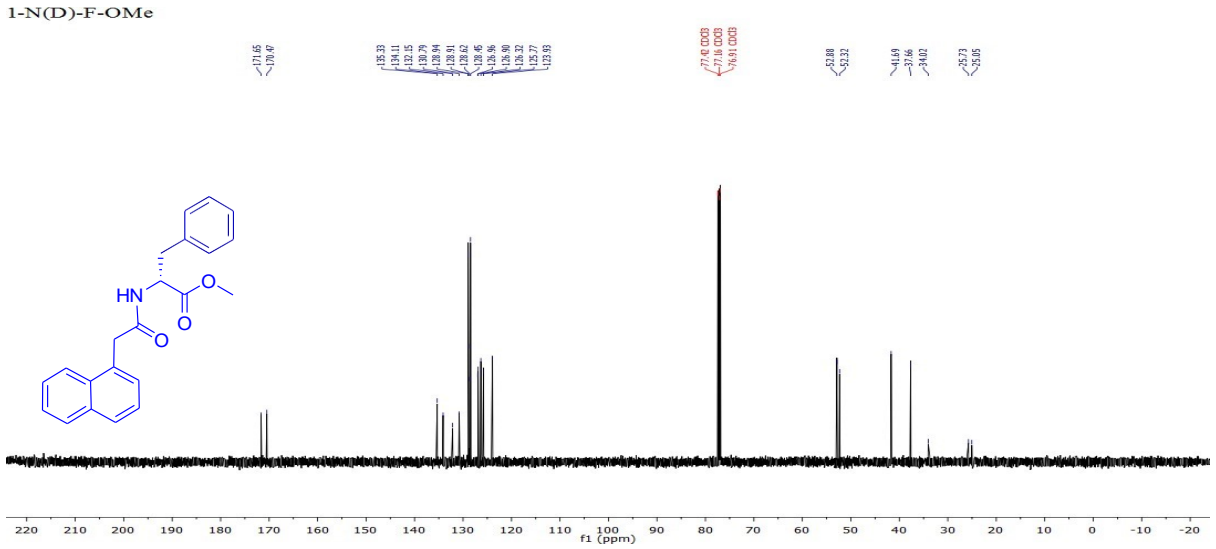

Figure S6. 125 MHz ^{13}C spectrum of ^{D}***N*ap-*F*-OMe.

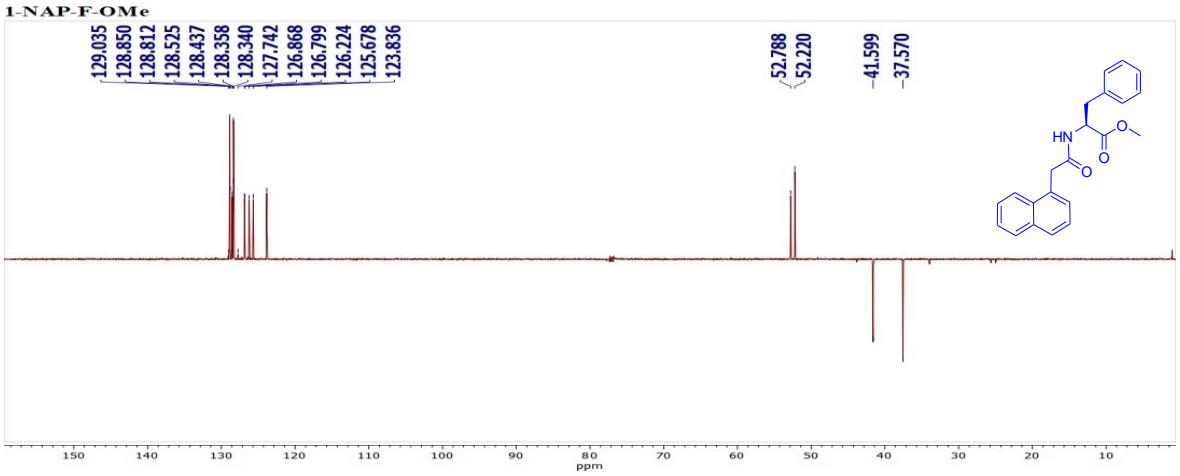

Figure S7. 125 MHz DEPT-135 NMR spectrum of ^{L}***N*ap-*F*-OMe.

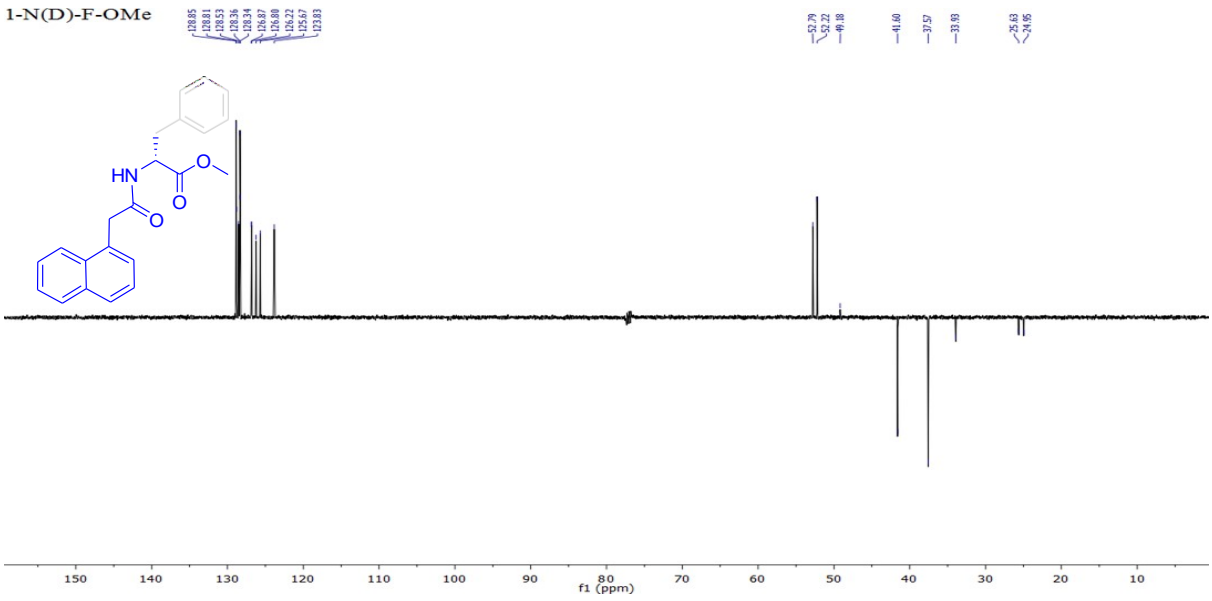

Figure S8. 125 MHz DEPT-135 NMR spectrum of ^{D}***N*ap-*F*-OMe.

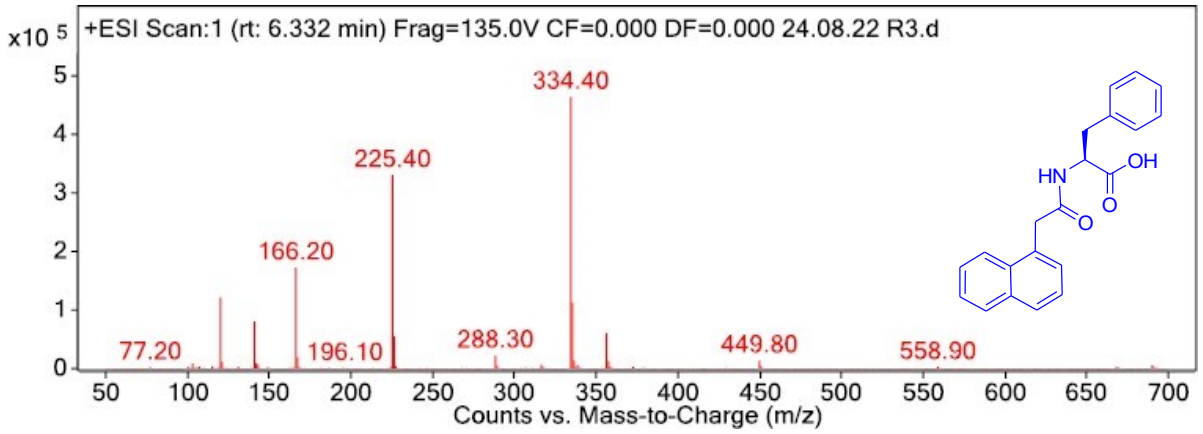

Figure S9. LC-MS-ESI spectrum of ^{L}***N*ap-*F*-OH.

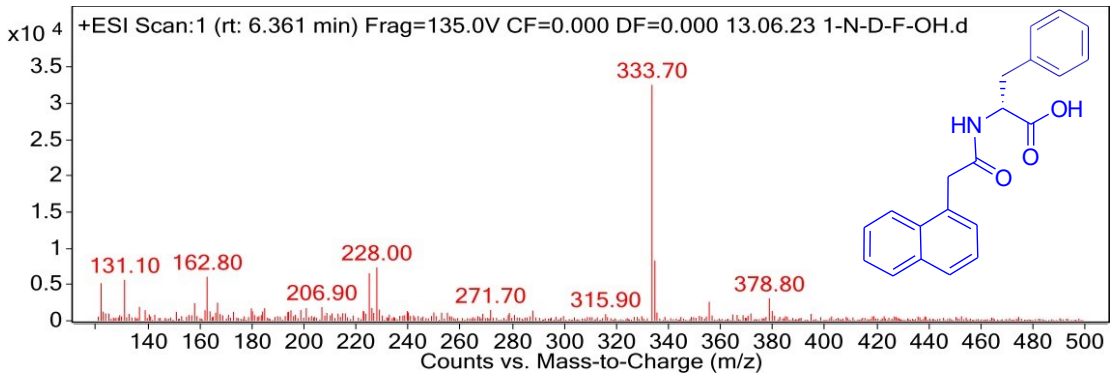

Figure S10. LC-MS-ESI spectrum of ^{D}***N*ap-*F*-OH.

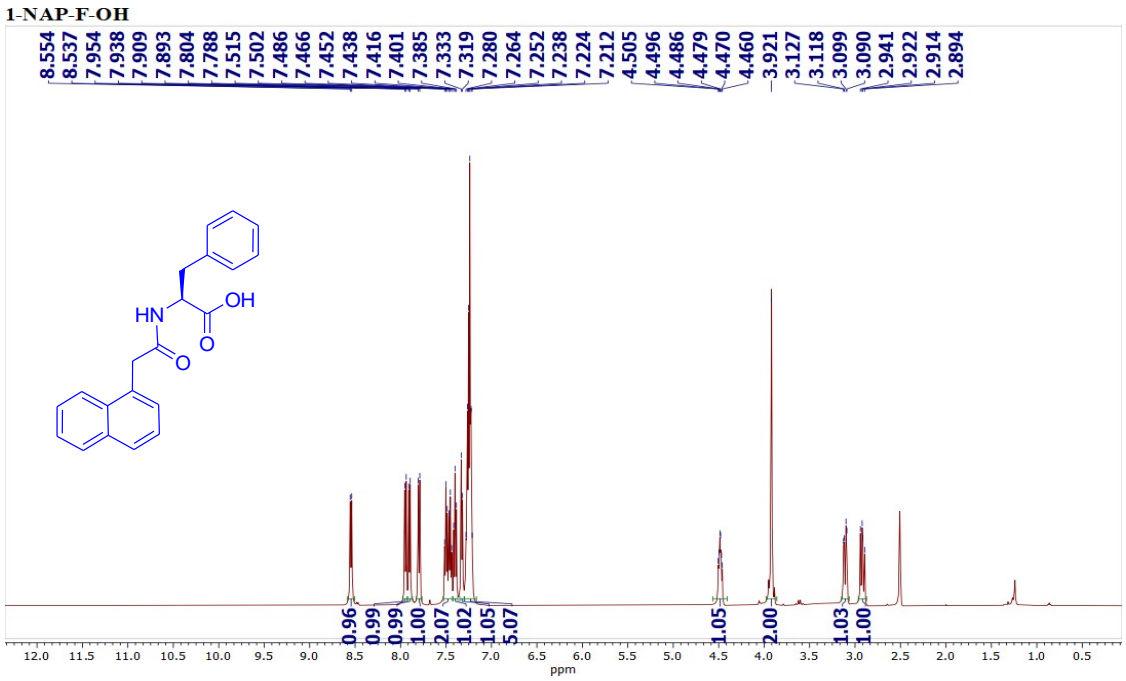

Figure S11. 500 MHz ^{1}H NMR spectrum of ^{L}***N*ap-*F*-OH.

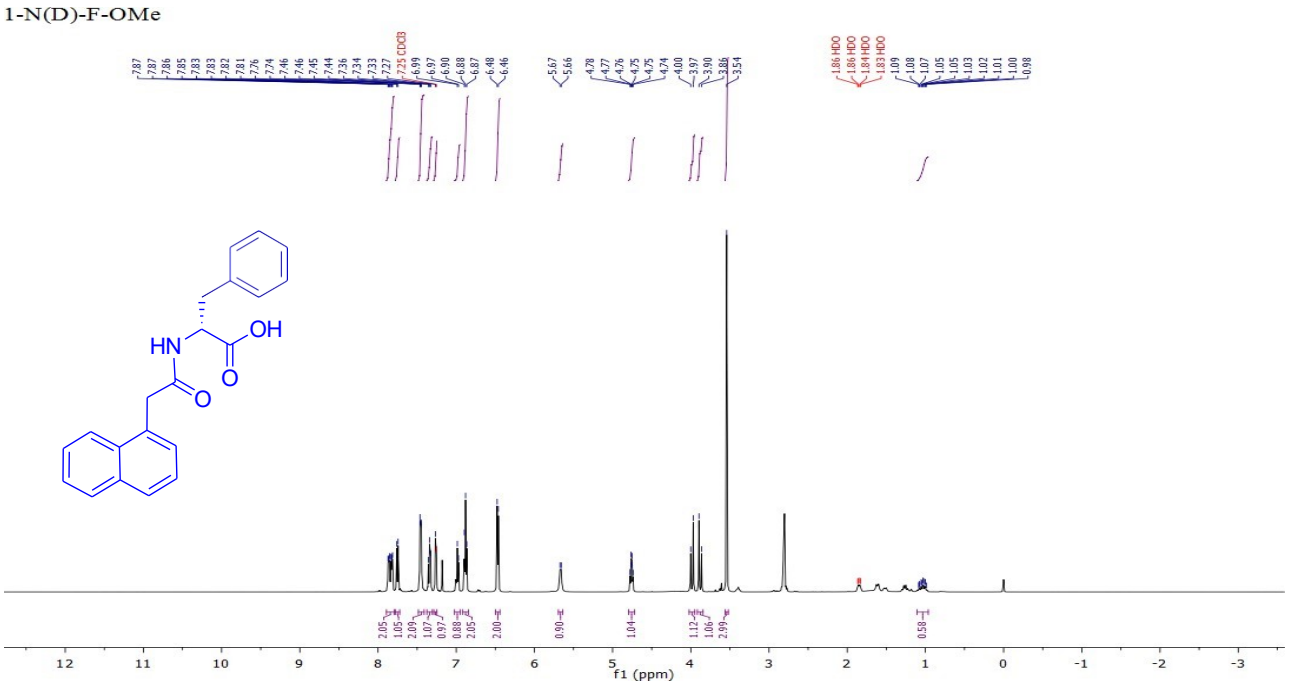

Figure S12. 500 MHz ^{1}H NMR spectrum of ^{D}***N*ap-*F*-OH.

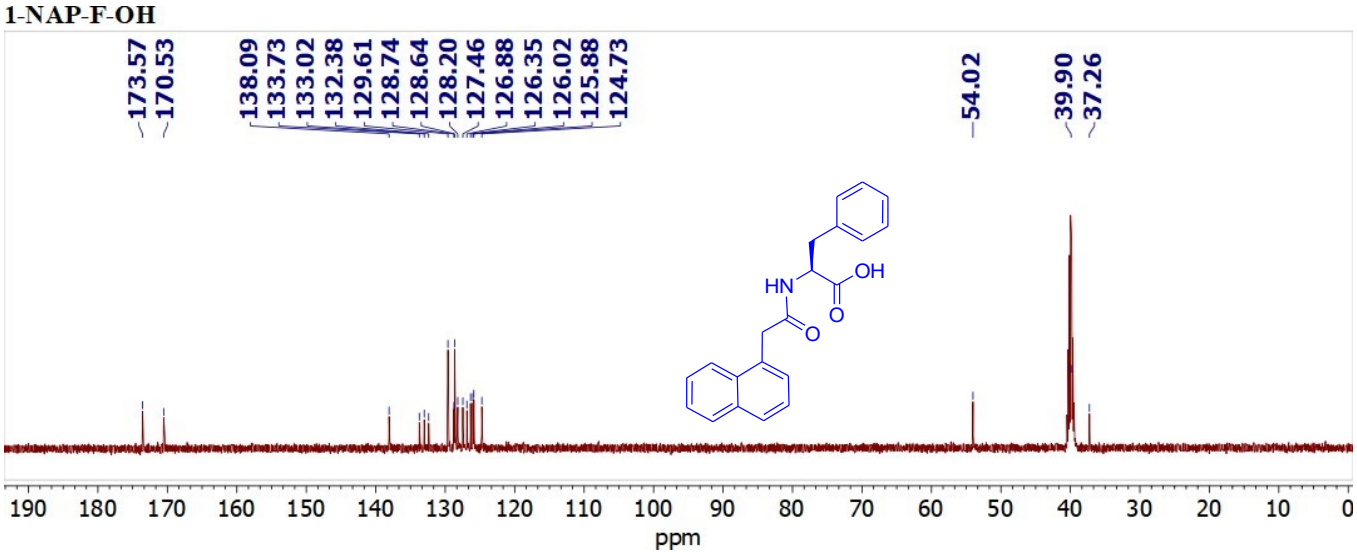

Figure S13. 125 MHz ^{13}C spectrum of ^{L}***N*ap-*F*-OH.

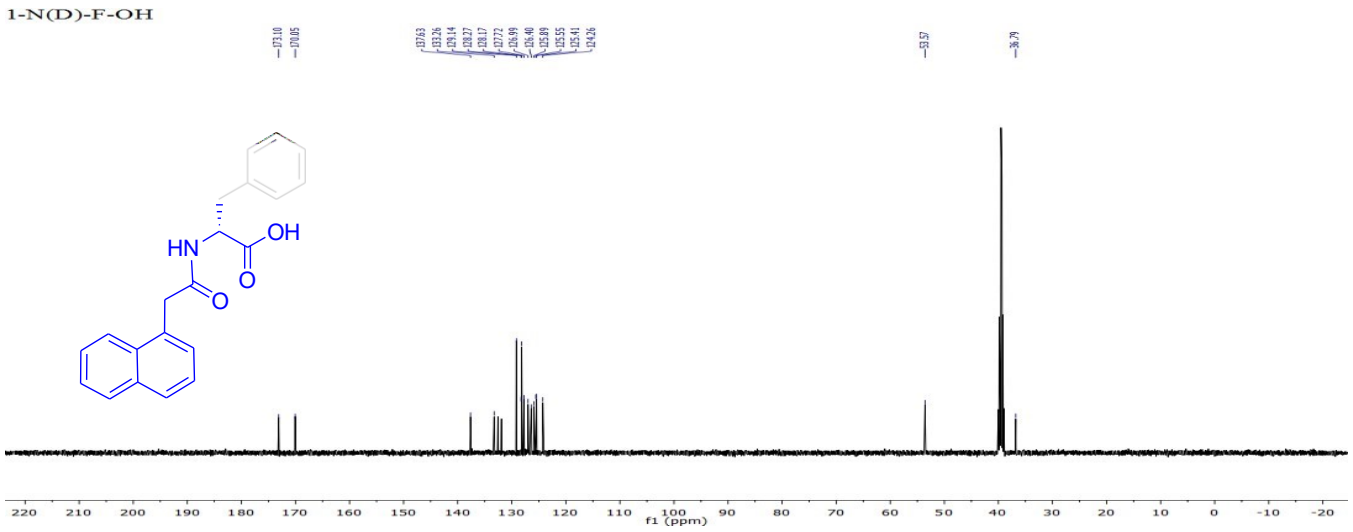

Figure S14. 125 MHz ^{13}C spectrum of ^{D}***N*ap-*F*-OH.

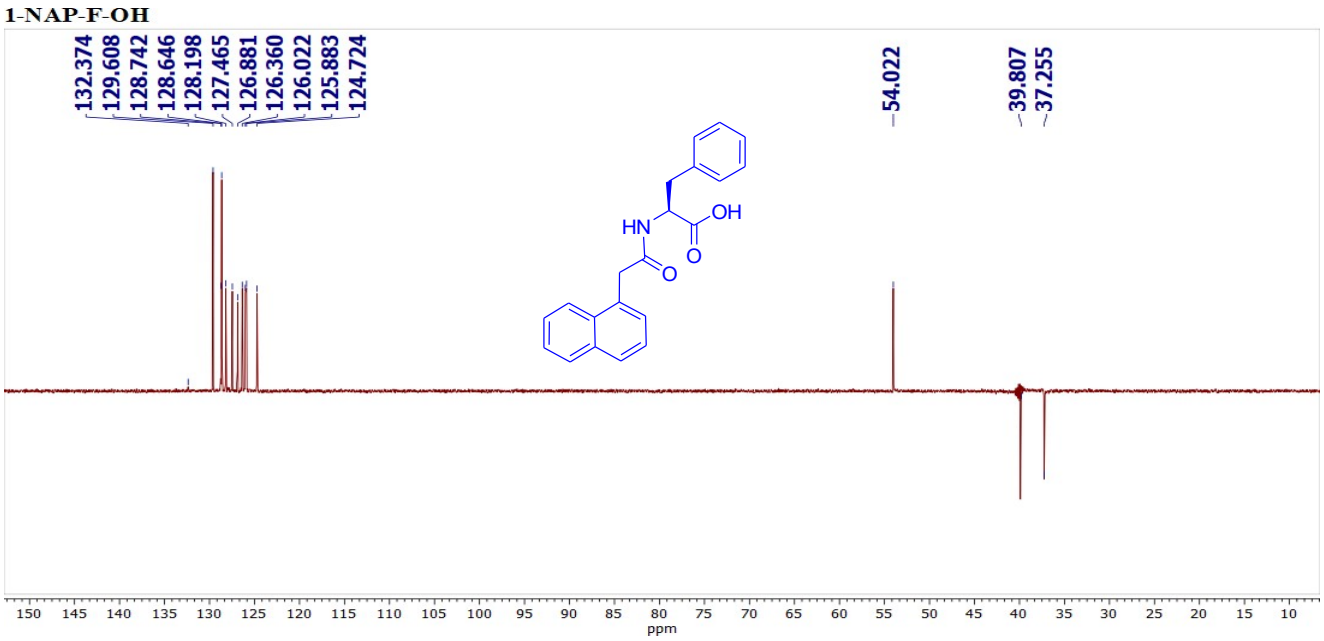

Figure S15. 125 MHz DEPT-135 NMR spectrum of ^{L}***N*ap-*F*-OH.

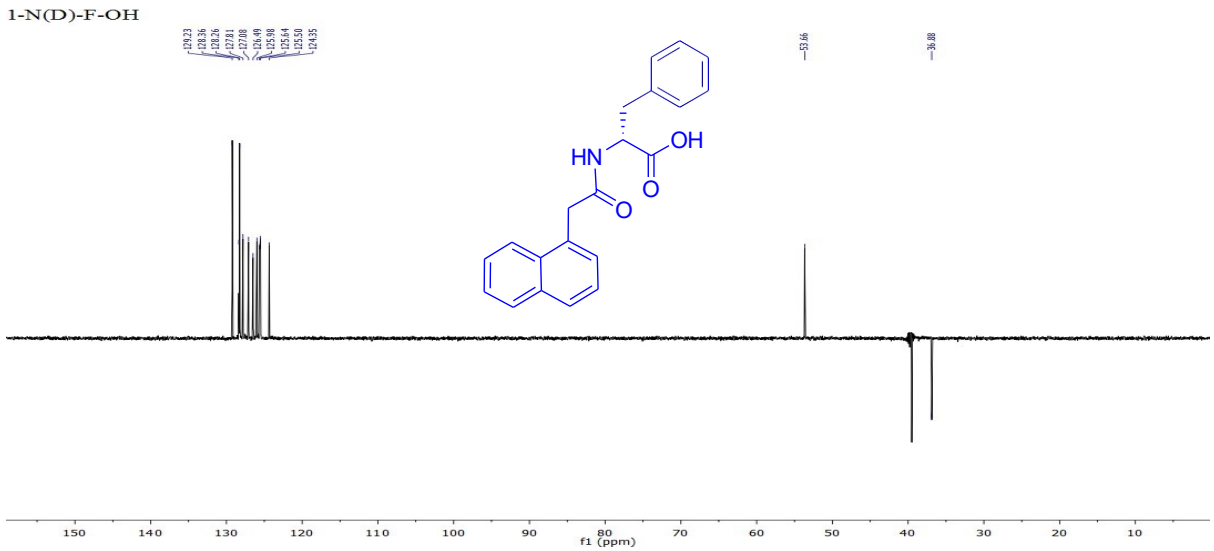

Figure S16. 125 MHz DEPT-135 NMR spectrum of ^{D}***N*ap-*F*-OH.

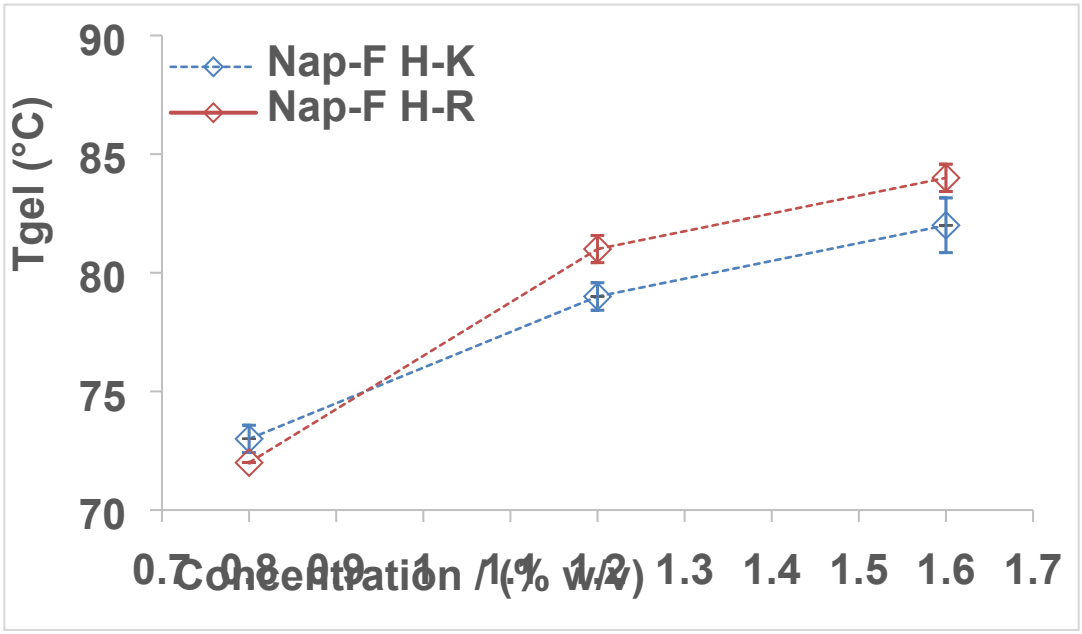

Figure S17. T_{gel} profile of the native **Nap-F$_{H-K}$** and **Nap-F$_{H-R}$** hydrogels. Error bars are shown inside the symbol as standard deviation.

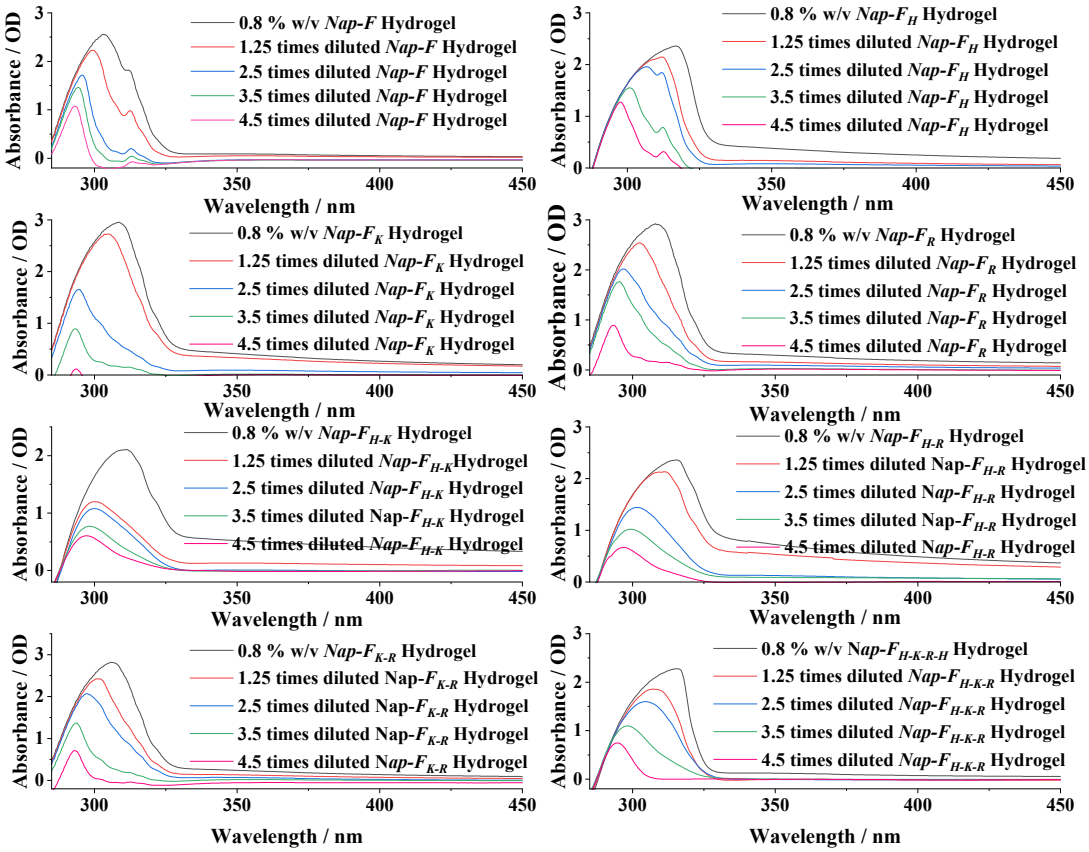

Figure S18. UV-Vis spectroscopic studies of the for mono (**Nap-F**), two (**Nap-F$_H$**, **Nap-F$_K$** and **Nap-F$_R$**), three (**Nap-F$_{H-K}$**, **Nap-F$_{H-R}$** and **Nap-F$_{K-R}$**) and four component (**Nap-F$_{H-K-R}$**) hydrogels and in their solutions states at different dilutions.

Table S1. X-ray diffraction major and minor peaks present for all the xerogels of mono (**Nap-F**), two (**Nap-F_H**, **Nap-F_K** and **Nap-F_R**), three (**Nap-F_{H-K}**, **Nap-F_{H-R}** and **Nap-F_{K-R}**) and four component (**Nap-F_{H-K-R}**) hydrogels in their assembled state.

	N*ap-*F	***N*ap-F_K**	***N*ap-F_{H-K}**	***N*ap-F_{K-R}**	***N*ap-F_{H-K-R}**	***N*ap-F_H**	***N*ap-F_R**	***N*ap-F_{H-R}**
2 θ/d (Å)	**7.75**/11.4 Highest Intensity	7.13/12.4	7.08/12.5	7.08/12.5	7.13/12.4	5.39/16.4	7.19/12.3	7.19/12.3
	9.44/9.4	7.71/11.5	9.46/9.3	7.78/11.4	8.76/10.1	7.31/12.1	7.71/11.5	9.05/9.8
	15.45/5.7	8.53/10.4	10.68/8.3 Low Intensity peak	8.53/10.4	9.46/9.3	8.24/10.7	8.53/10.4	9.46/9.3
	17.35/5.1	10.57/8.4 Medium Intensity	15.16/5.8	10.63/8.3 Highest Intensity	9.87/9.0	9.46/9.3	9.46/9.3	9.93/8.9
	17.98/4.9	17.08/5.2 Highest Intensity	17.43/5.1	15.51/5.7	10.68/8.3	10.98/8.1 Low Intensity peak	10.57/8.4 Medium Intensity	10.86/8.1
	19.92/4.5	18.31/4.8	18.89/4.7 Medium Intensity	17.08/5.2 Medium Intensity	15.28/5.8	14.06/6.3	12.26/7.2	14.46/6.1
	23.26/3.8	21.39/4.2	21.16/4.2 Highest Intensity	17.38/5.1	15.81/5.6	14.70/6.0	14.41/6.1	15.28/5.8
	28.60/3.1	21.98/4.0	23.89/3.7 Medium Intensity	18.31/4.8	17.55/5.1	15.34/5.8 Low Intensity peak	17.08/5.2 Highest Intensity	16.68/5.3
		22.38/4.0	28.61/3.1	21.39/4.2	18.13/4.9	18.95/4.7 Medium Intensity	18.31/4.8	17.5/5.1
		24.59/3.6	29.77/3.0	21.98/4.0	18.95/4.7 Highest Intensity	21.16/4.2 Low Intensity peak	20.22/4.4	19.01/4.7 Medium Intensity
		28.73/3.1		22.45/4.0	21.10/4.2 Highest Intensity	24/3.7 Highest Intensity	20.75/4.3	19.94/4.5
				24.65/3.6	24.01/3.7 Highest Intensity	27.97/3.2	21.16/4.2	20.52/4.3
				28.20/3.2	28.66/3.1	28.66/3.1	21.45/4.1	21.16/4.2 Highest Intensity
					29.89/3.0	29.48/3.0	22.03/4.0	24.13/3.7 Highest Intensity
						29.89/3.0	22.44/4.0	25.41/3.5
							24.59/3.6	26.46/3.4
							28.66/3.1	29.13/3.1
							29.77/3.0	29.89/3.0

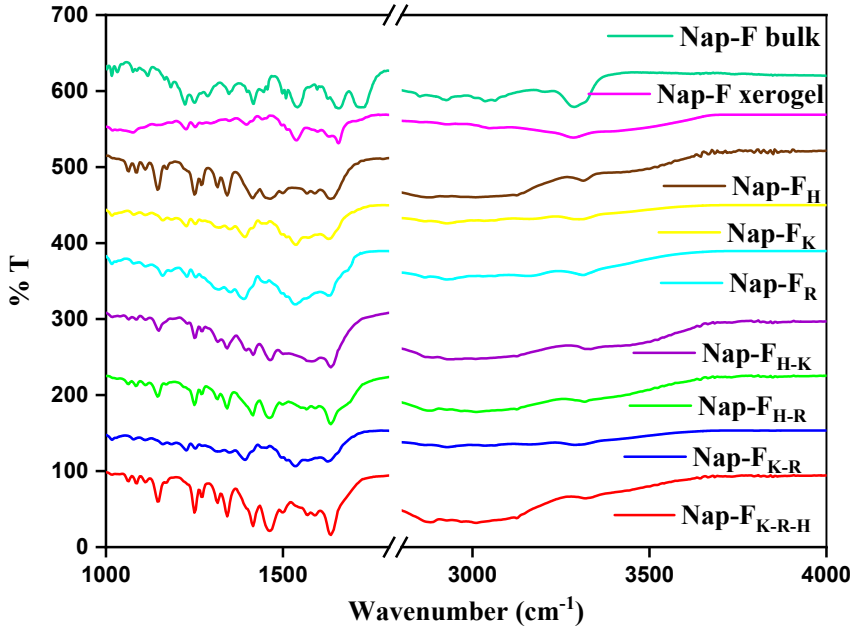

Figure S19. FT-IR spectra of **Nap-F** bulk, mono (**Nap-F**), two (**Nap-F$_H$**, **Nap-F$_K$** and **Nap-F$_R$**), three (**Nap-F$_{H-K}$**, **Nap-F$_{H-R}$** and **Nap-F$_{K-R}$**) and four components (**Nap-F$_{H-K-R}$**) xerogels in KBr.

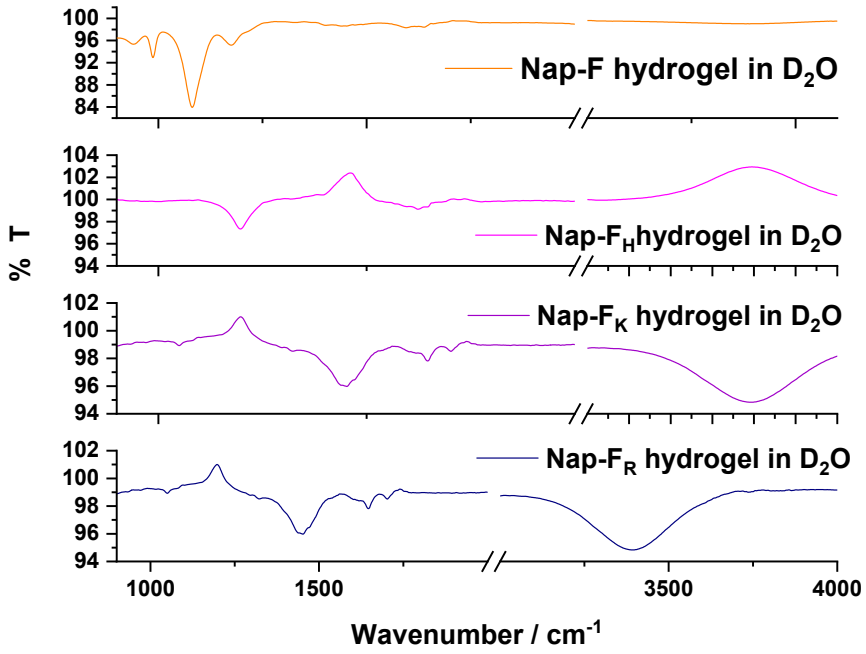

Figure S20. FTIR-ATR spectra of ***Nap-F*** bulk and two **Nap-F$_H$**, **Nap-F$_K$** and **Nap-F$_R$** hydrogels in D_2O.

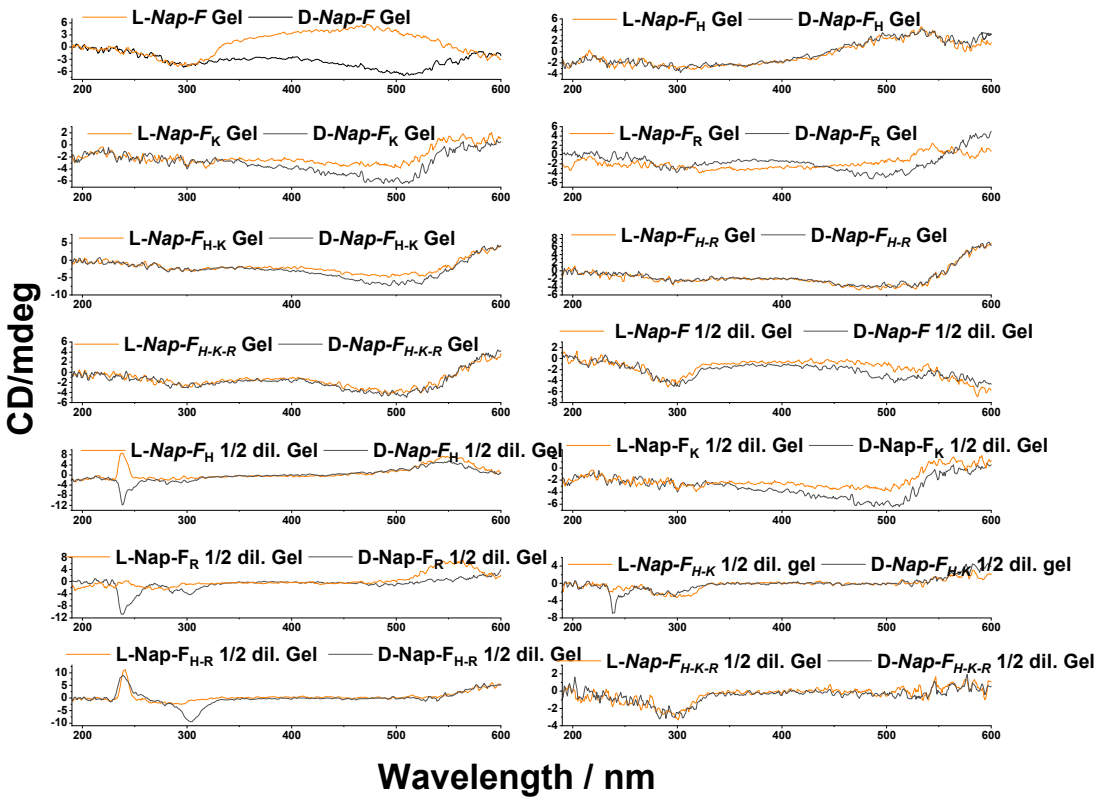

Figure S21. Circular Dichroism spectroscopic responses of the mono (**Nap-F**), two (**Nap-F$_H$, Nap-F$_K$ and Nap-F$_R$**), three (**Nap-F$_{H-K}$, Nap-F$_{H-R}$ and Nap-F$_{K-R}$**) and four-component (**Nap-F$_{H-K-R}$**) hydrogels at 0.8 % w/v concentrations and half diluted hydrogels for both L-and D-amino acids-based assembled systems.

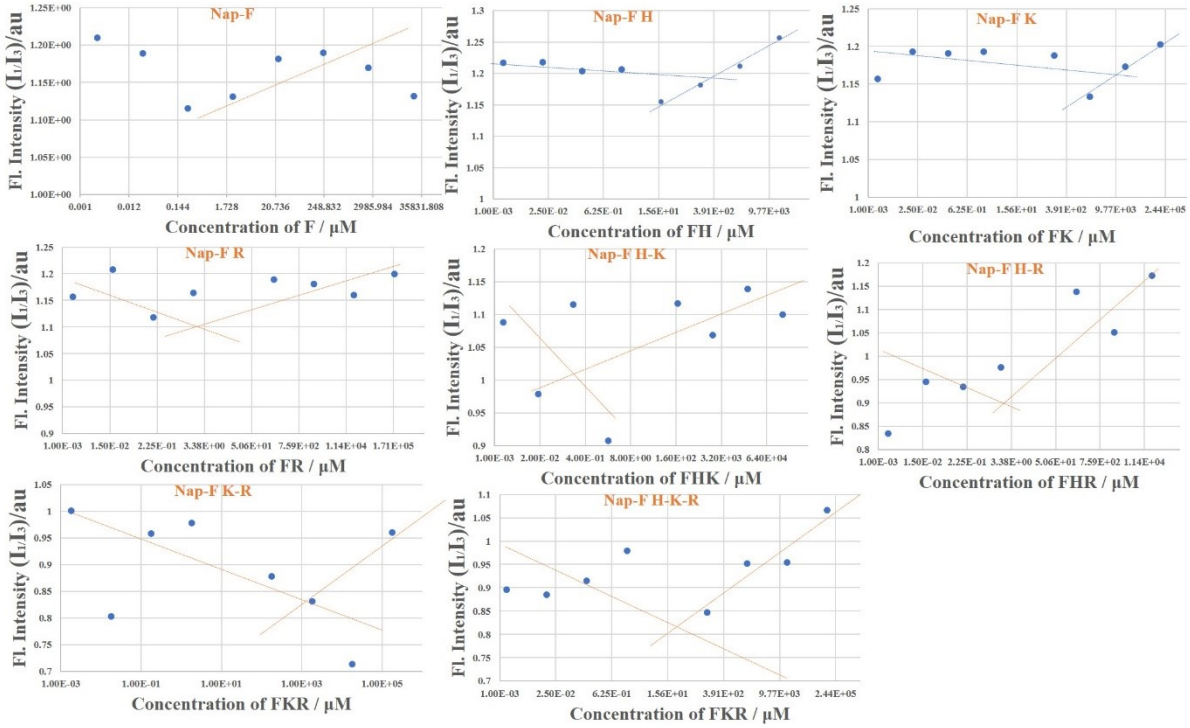

Figure S22. Responses of I_1/I_3 in the pyrene emission spectra as a function of the concentration of the native, two-, three- and four-component assembled systems. Pyrene concentration kept at 10^{-6} M in all the measurements.

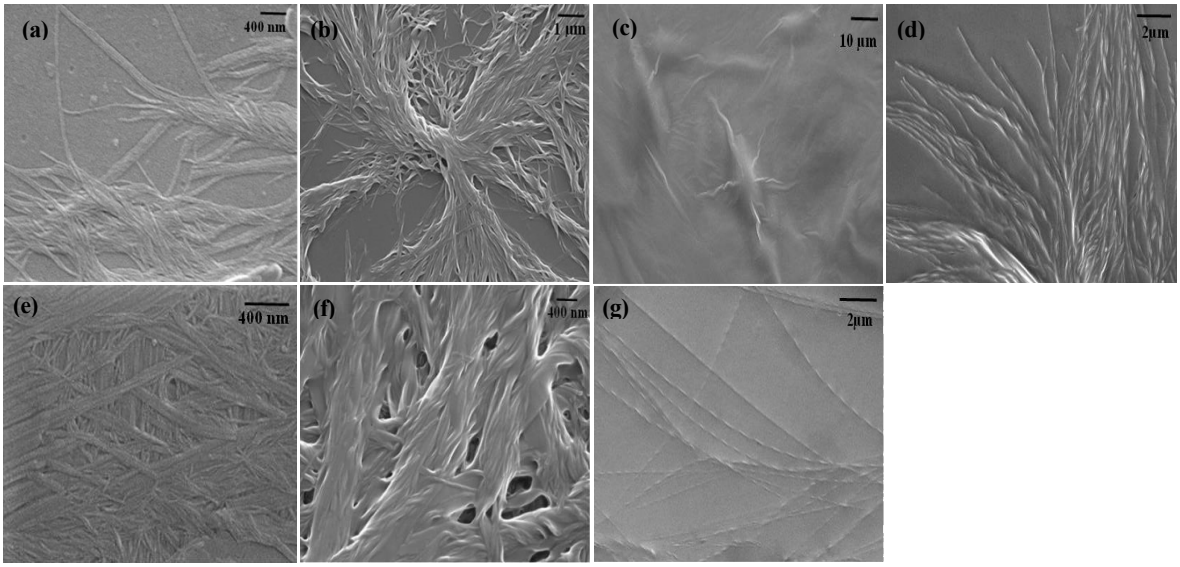

Figure S23. FE-SEM images at assembled solutions (50 times dilution for all samples done from 0.5 w/v % co- assembled solution) which have been used for catalytic studies **(a) Nap-F_H** 2.5:2.5, **(b) Nap-F_K** 2.5:2.5, **(c) Nap-F_R** 2.5:2.5 (0.5 w/v %), **(d) Nap-F_{H-K}** 3:1:1, **(e) Nap-F_{H-R}** 3:1:1 **(f) Nap-F_{K-R}** 3:1:1, **(g) Nap-F_{H-K-R}** 2:1:1:1.

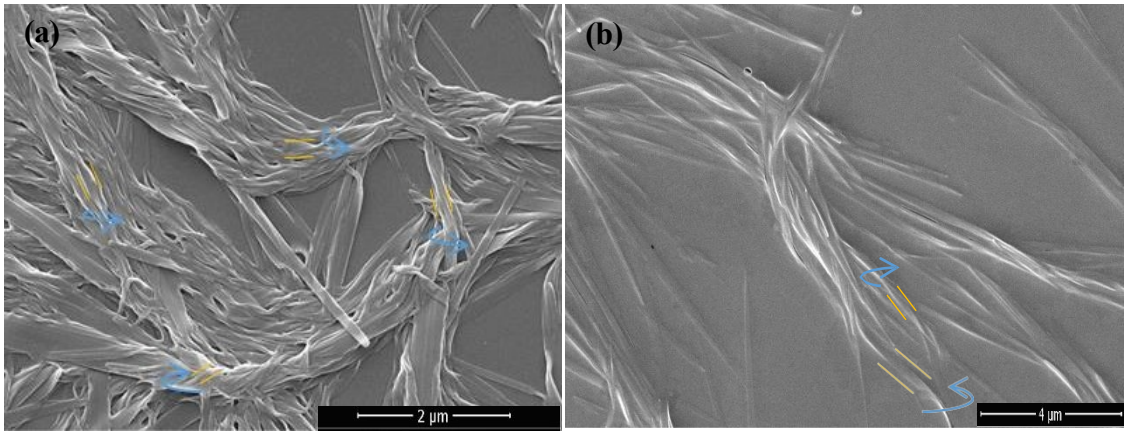

Figure S24. FE-SEM images at assembled solutions of **(a)** ^{D}**Nap-F_K** and **(b)** ^{D}**Nap-F_{K-R}** after 50 times dilution at 0.01 % w/v concentrations.

Table S2. Handedness of the helical fibers.

Catalytic system	Total strands	Right-handed	left-handed
^{L}***Nap-F$_K$***	250	100 %	0
^{L}***Nap-F$_{H-K}$***	70	100%	0
^{L}***Nap-F$_{K-R}$***	140	100%	0
^{L}***Nap-F$_{H-K-R}$***	90	100%	0
^{D}***Nap-F$_K$***	210	20%	80%
^{D}***Nap-F$_{K-R}$***	100	10%	90%

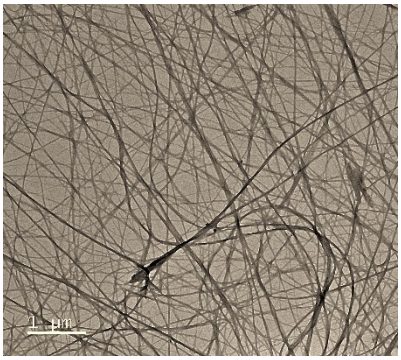

Figure S25. TEM image of **Nap-F$_{K-R}$** showing helical twisted fibers.

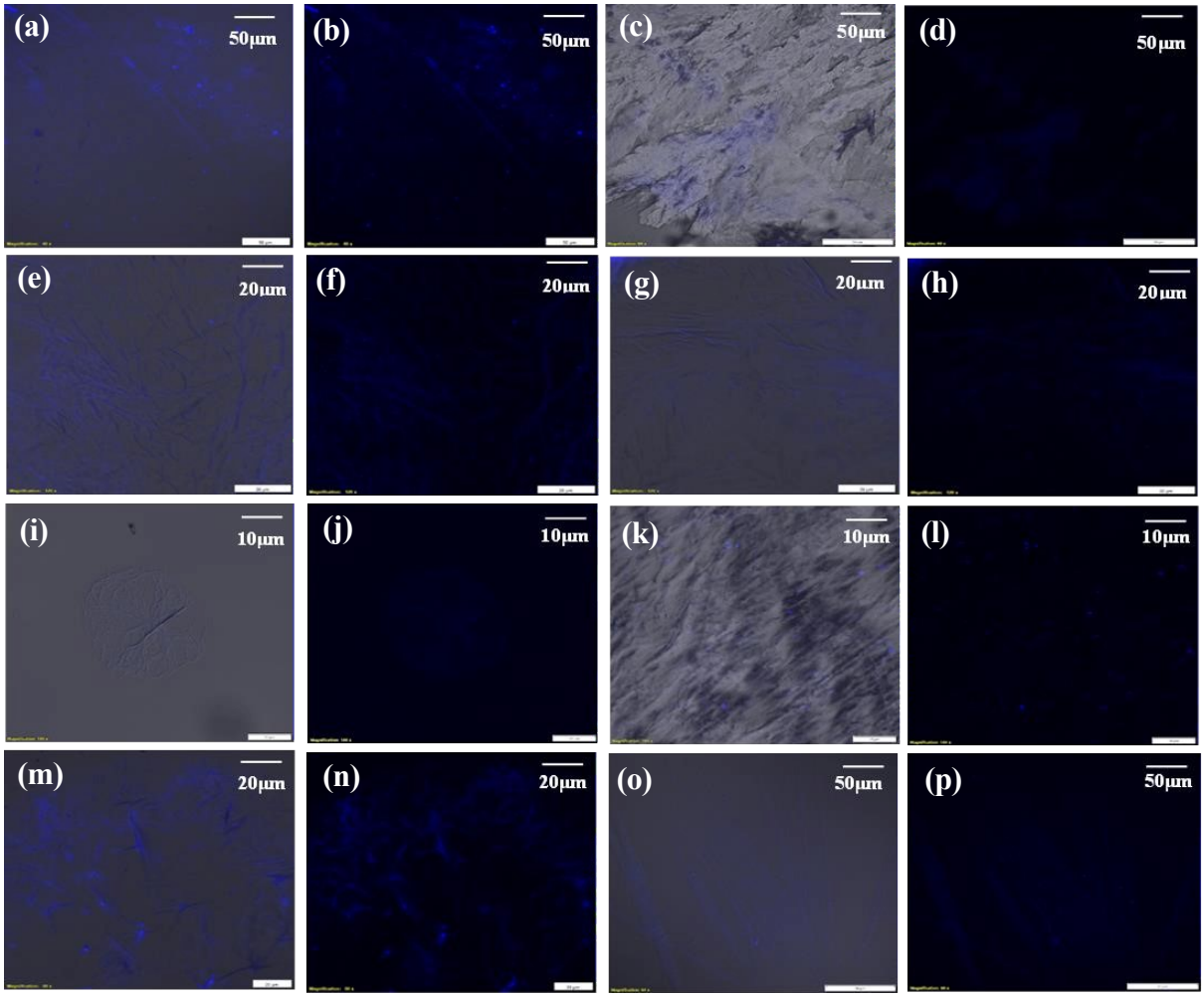

Figure S26. Confocal microscopic images of the hydrogels at 0.8 w/v % concentrations **(a)** & **(b)** for **Nap-F**; **(c)** & **(d)** for **Nap-F$_H$** (6:2); **(e)** & **(f) Nap-F$_K$** (6:2)**; (g)** & **(h)** for **Nap-F$_R$** (6:2); **(i)** & **(j)** for **Nap-F$_{H-K}$** (6:1:1); **(k)** & **(l)** for **Nap-F$_{H-R}$** (6:1:1)**; (m)** & **(n) Nap-F$_{K-R}$** (6:1:1) and **(o)** & **(p)** for **Nap-F$_{H-K-R}$** (5:1:1:1) under bright field and dark field at **405 nm** respectively.

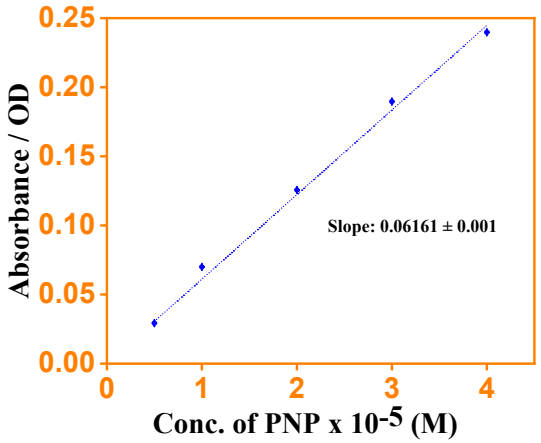

Figure S27. Absorbance vs Concentration plot for determination of molar extinction coefficient (ε) of *p*- nitrophenol in water.

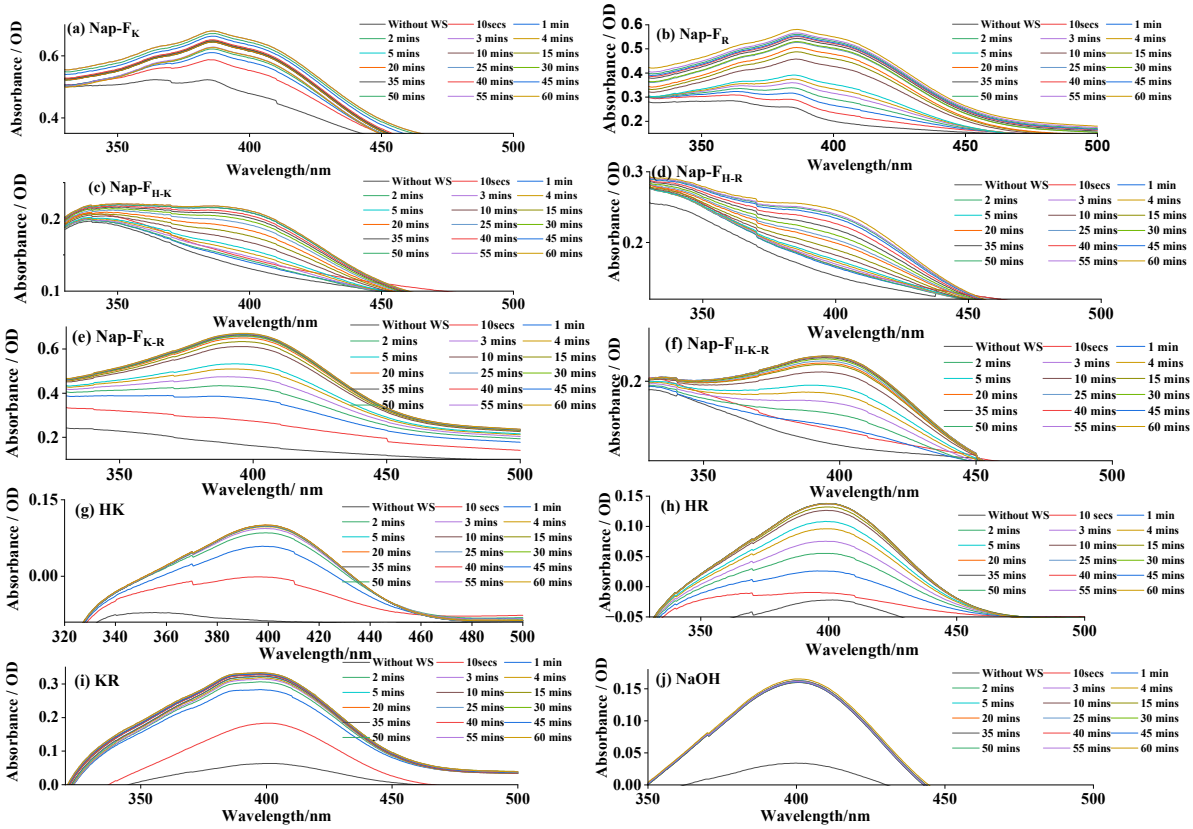

Figure S28. The progress of the *p*-**NPA** to *p*-**NP** hydrolysis reaction monitored by time dependent UV-Vis spectroscopic study for the systems including a) **H-K**, (b) **H-R**, (c) **K-R**, (d) **Nap-F$_{K}$**, (e) **Nap-F$_{R}$**, (f) **Nap-F$_{H-K}$**, (g) **Nap-F$_{H-R}$**, (h) **Nap-F$_{K-R}$**, (i) **Nap-F$_{H-K-R}$** and (j) **NaOH**.

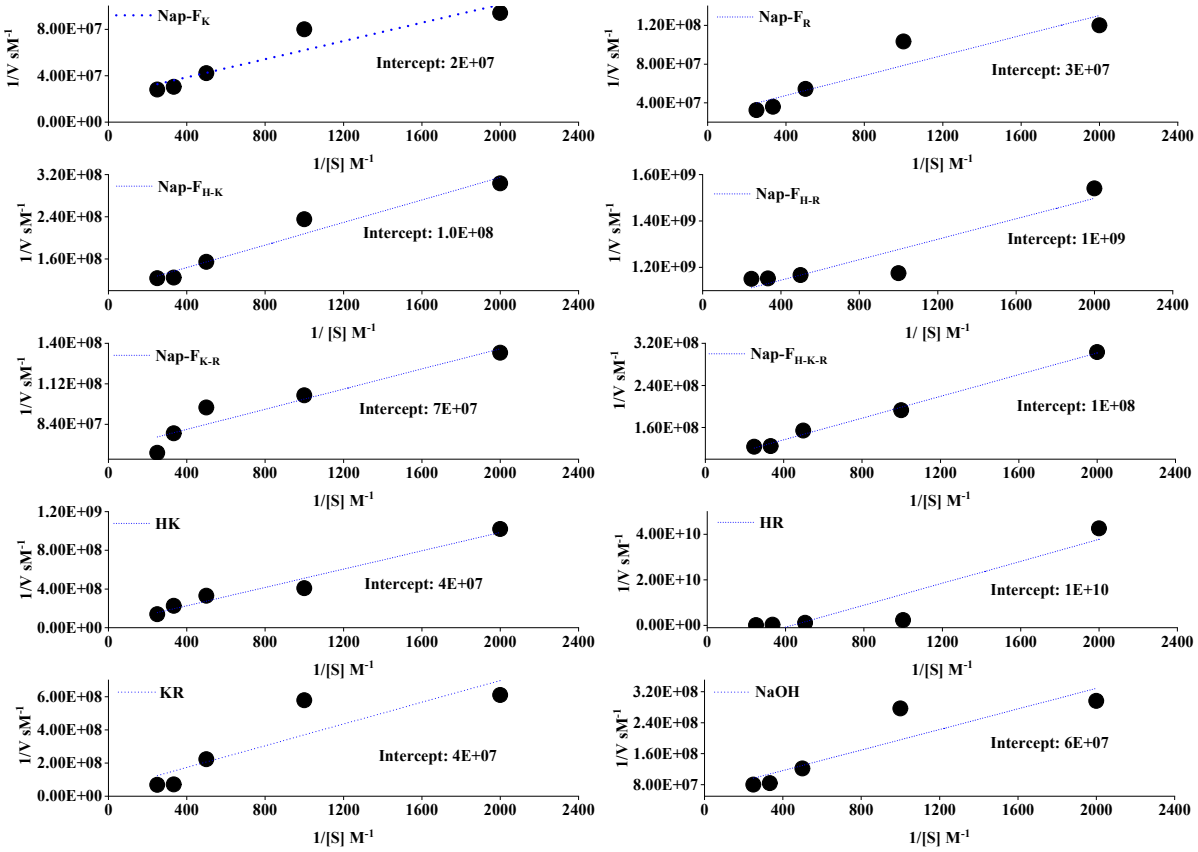

Figure S29. Lineweaver-Bruk plot for the hydrolysis of *p*-**NPA** by using various systems as catalysts such as **H-K**, **H-R**, **K-R**, Nap-F$_{\mathbf{K}}$, Nap-F$_{\mathbf{R}}$, Nap-F$_{\mathbf{H\text{-}K}}$, Nap-F$_{\mathbf{H\text{-}R}}$, Nap-F$_{\mathbf{K\text{-}R}}$, Nap-F$_{\mathbf{H\text{-}K\text{-}R}}$ and **NaOH**.

Table S3. Kinetic parameters for the hydrolysis of PNPA in the presence of different catalyst systems in water. The Michaelis–Menten kinetics equation $v = \frac{d[P]}{dt} = \frac{K_{cat}}{K_m}[E]_0[S]$ and double-reciprocal (Lineweaver–Burk) method with the equation $v = \frac{d[P]}{dt} = K_{cat}[E]_0\frac{[S]}{K_M + [S]}$ were used where v is reaction rate, [P] is concentration of product, $[E]_0$ is the initial enzyme concentration, [S] is substrate (p-nitrophenyl acetate) concentration, k_{cat} is the catalytic rate constant, and K_M is the Michaelis constant. The k_{cat}/K_M values calculated from the linear fitting of the double-reciprocal (Lineweaver–Burk) plot (Figure S29).

Catalyst	K_{cat} (s^{-1})	K_M (M)	K_{cat} / K_M (M^{-1} s^{-1})
H-K (2.5:2.5) (0.5% w/v)	1.52×10^{-4}	1.18×10^{-2}	**1.28×10^{-2}**
H-R (2.5:2.5) (0.5% w/v)	6.06×10^{-7}	2.00×10^{-3}	**3.03×10^{-4}**
K-R (2.5:2.5) (0.5% w/v)	1.67×10^{-4}	8.19×10^{-3}	**2.03×10^{-2}**
Nap-F$_K$ (2.5:2.5) (0.5% w/v)	4.80×10^{-4}	1.96×10^{-3}	**2.45×10^{-1}**
Nap-F$_R$ (2.5:2.5) (0.5% w/v)	3.38×10^{-4}	1.72×10^{-3}	**1.96×10^{-1}**
Nap-F$_{H-K}$ (3:1:1) (0.5% w/v)	1.81×10^{-4}	2.26×10^{-3}	**8.02×10^{-2}**
Nap-F$_{H-R}$ (3:1:1) (0.5% w/v)	1.35×10^{-5}	2.20×10^{-4}	**6.14×10^{-2}**
Nap-F$_{K-R}$ (3:1:1) (0.5% w/v)	1.87×10^{-4}	4.97×10^{-3}	**3.76×10^{-1}**
Nap-F$_{H-K-R}$ (2:1:1:1) (0.5% w/v)	1.62×10^{-4}	1.07×10^{-3}	**1.51×10^{-1}**
NaOH (0.5% w/v)	**1.33×10^{-4}**	**2.21×10^{-3}**	**6.03×10^{-2}**

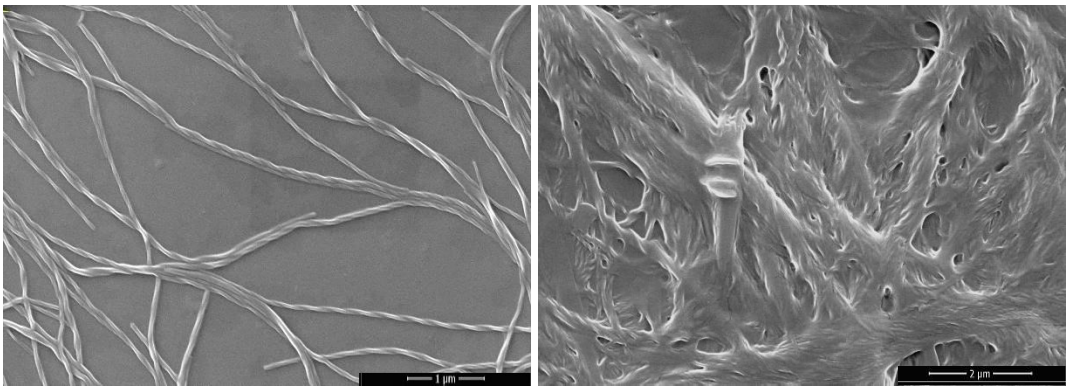

Figure S30. FE-SEM of **(a) Nap-F$_K$** and **(b) Nap-F$_{K-R}$** after the catalysis suggesting the stability of the co-assembles structures.

Table S4. pHs of the assembled systems after the before and *p*-PNPA hydrolysis.

Catalytic systems	pH before catalysis in water	pH after catalysis in water	Amt. of I (N) NaOH / HCl added to make pH 9	pH after catalysis from pH-9
Nap-F$_H$	5.97	6.0	100ul	8.58
Nap-F$_K$	8.94	9.00	5ul	8.04
Nap-F$_R$	8.74	8.84	20ul	8.40
Nap-F$_{H-K}$	5.82	6.35	60ul	7.83
Nap-F$_{H-R}$	5.37	6.11	70ul	8.3
Nap-F$_{K-R}$	7.8	8.5	50ul	7.8
Nap-F$_{H-K-R}$	8.49	8.3	20ul	8.6
H-K-R	9.25	9.27	13ul (HCl)	8.74
H-K	8.87	9.05	10ul	8.57
H-R	8.69	8.88	12ul	8.64
K-R	9.79	9.95	5ul (HCl)	8.68

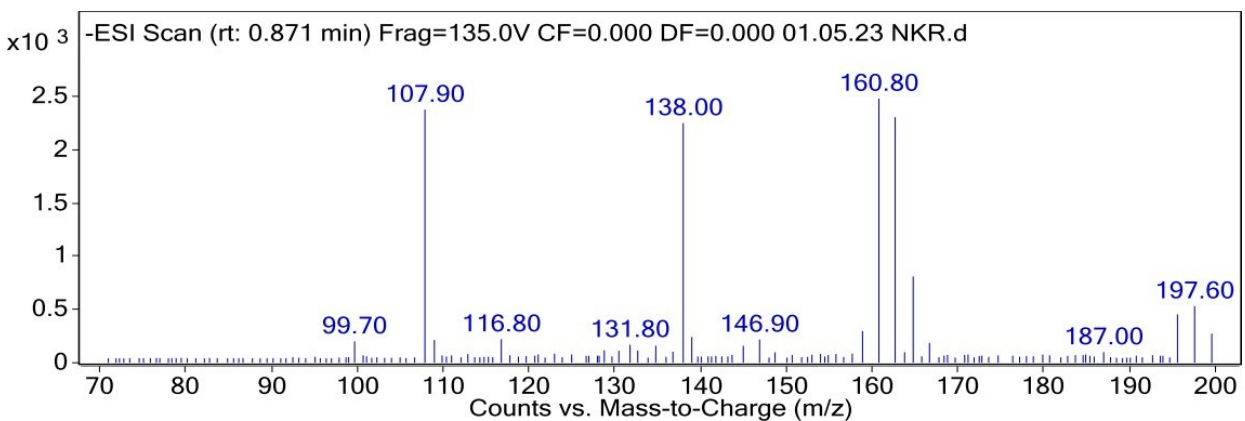

Hydrolysis performed using the catalytic systems at positive mode ESI	Peaks found at m/z	Possible molecular ion and fragments corresponding to the m/z
NaOH both at 50 and 70 V (Figure S31)	107	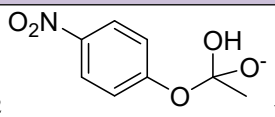 m/z at 107 is due to $[M+2H_2O+2H^+]/2$ $+H_2O+2H]^{2+}$
	117	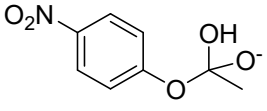 m/z at 117 is due to $[198+2NH_4^+]/2$ $+2NH_4^+]^{2+}$
	122	m/z at 122 due to [M+2Na]/2 of the intermediate shown below when hydroxyl ions act as nucleophile 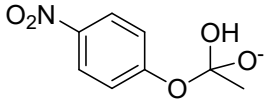 $+2Na]^{2+}$
	139	m/z at 139 is due to $M_{PNP}]^+$
Histidine (H) only at 50 and 70 V (Figure S32)	107	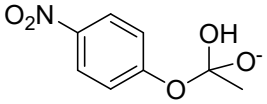 m/z at 107 is due to $[M+2H_2O+2H^+]/2$ as $+H_2O+2H]^{2+}$
	117	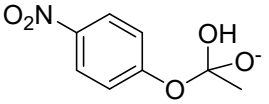 m/z at 117 is due to $[198+2NH_4^+]/2$ as $+2NH_4^+]^{2+}$
	156	m/z at 156 is due to $[M_{Histidine}+H]^+$
Lysine (K) only at 50 and 70 V (Figure S33)	107	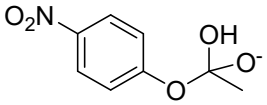 m/z at 107 is due to $[M+2H_2O+2H^+]/2$ as $+H_2O+2H]^{2+}$
	117	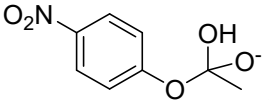 m/z at 117 is due to $[198+2NH_4^+]/2$ as $+2NH_4^+]^{2+}$
	147	m/z at 147 $[M_{Lysine}+H]^+$
Arginine (R) only at 50 and 70 V (Figure S34)	175	m/z at 175 is due to $[M_{Arginine}+H]^+$
	117	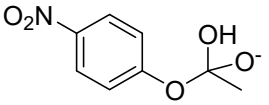 m/z at 117 is due to $[198+2NH_4^+]/2$ as $+2NH_4^+]^{2+}$
	276	Diacetyl arginine$+H_2O]^+$

Figure S31. ESI-MS of the catalytic mixture solution by **Nap-F$_{K-R}$** showing the corresponding molecular ion peak for *p*-nitrophenolate at m/z 138 and with one sodium ion at m/z 160.80. The peak at m/z 99.70 is originating may be form the acetic acid with one potassium ion. The peak at m/z 197.60 to 199 may be due to the formation of alkoxide ion intermediate (molar mass of the intermediate is 198 g mol^{-1}) due to the ester hydrolysis by hydroxyl as nucleophile.

Table S5: LC-ESI-MS analyses of the mass peaks obtained shown in Figure S31-41 in positive mode at lower voltages including 50 and 70 V.

Two (**Nap-F_H**, **Nap-F_K** and **Nap-F_R**), three (**Nap-F_{H-K}**, **Nap-F_{H-R}** and **Nap-F_{K-R}**) and four-component (**Nap-F_{H-K-R}**) **systems** (Figure S35 to 41)	225	m/z at 225 may be due to $[M_{Nap-F}+PNPA+2NH_4^+]/2$ or $[M_{Nap-F}+PNP+2K^+]/2$
	268	m/z at 225 may be due to or $[M_{Nap-F}+PNP+H_2O+2Na^+]/2$
	334	m/z at 334 may be due to M of the intermediate shown below when hydroxyl ions act as nucleophile 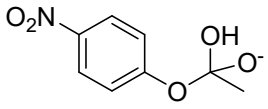 $+AcOH+2H_2O+K]^+$ or m/z at 334 can be due to the molecular ion peak along with one hydrogen of **Nap-F,** $[M_{Nap-F}+H]^+$
	356	m/z at 356 can be for $[M_{Nap-F}+Na]^+$
For **K** containing co-assembled two (**Nap-F_K**), three (**Nap-F_{H-K}** and **Nap-F_{K-R}**) and four-component (**Nap-F_{H-K-R}**) systems (Figure S36, 38, 40 to 41)	334	m/z at 334 can be for $[M_{Nap-F}+H]^+$
For **R** containing co-assembled Two (**Nap-F_R**), three (**Nap-F_{H-R}** and **Nap-F_{K-R}**) and four-component (**Nap-F_{H-K-R}**) systems (Figure S37, 39, 40 to 41)	334	m/z at 334 can be for $[M_{Nap-F}+H]^+$ or it can be $[M_{di\text{-}acetyl\ arginine}+K+2H_2O]^+$
For **H** containing co-assembled two (**Nap-F_H**), three (**Nap-F_{H-K}** and **Nap-F_{H-R}**) and four-component (**Nap-F_{H-K-R}**) systems (Figure S35, 38, 39 and 41)	334	m/z at 334 can be for $[M_{Nap-F}+H]^+$

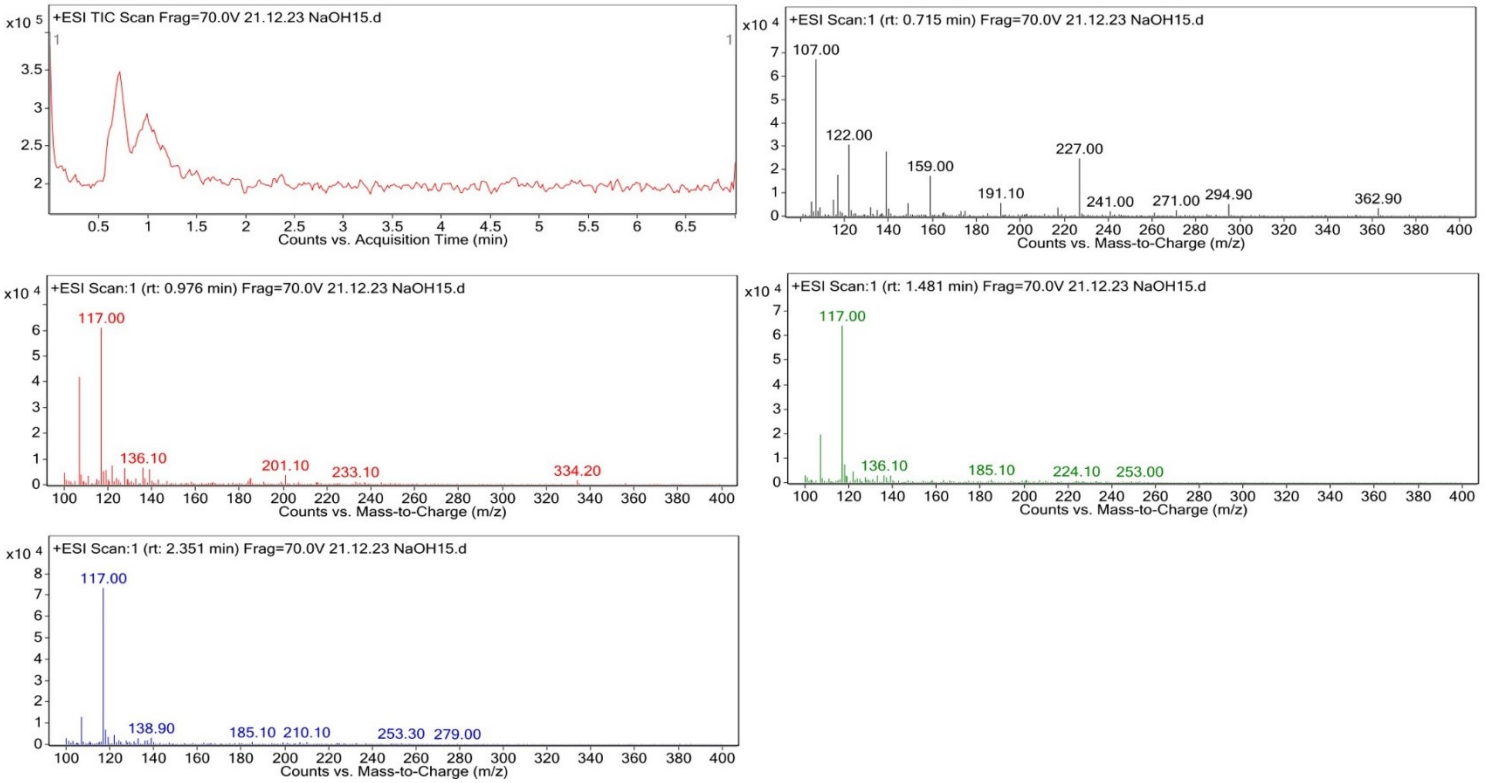

Figure S32. ESI-LC-MS profiles of the catalytic mixture solution by using NaOH.

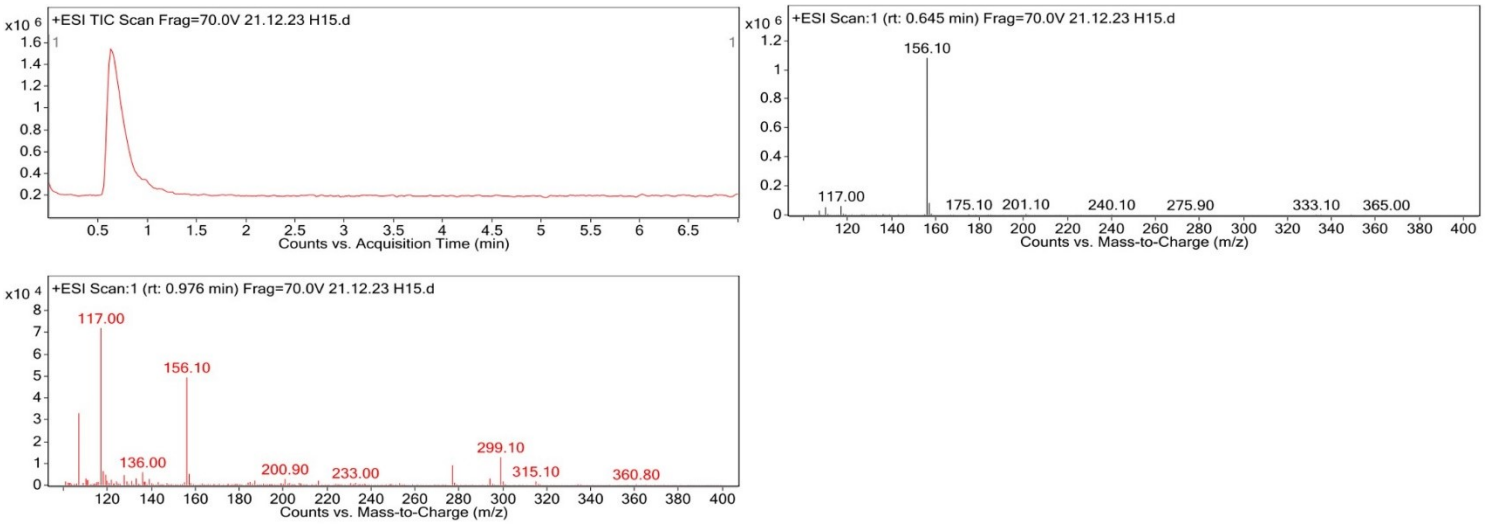

Figure S33. ESI-LC-MS profiles of the catalytic mixture solution by using basic amino acid histidine.

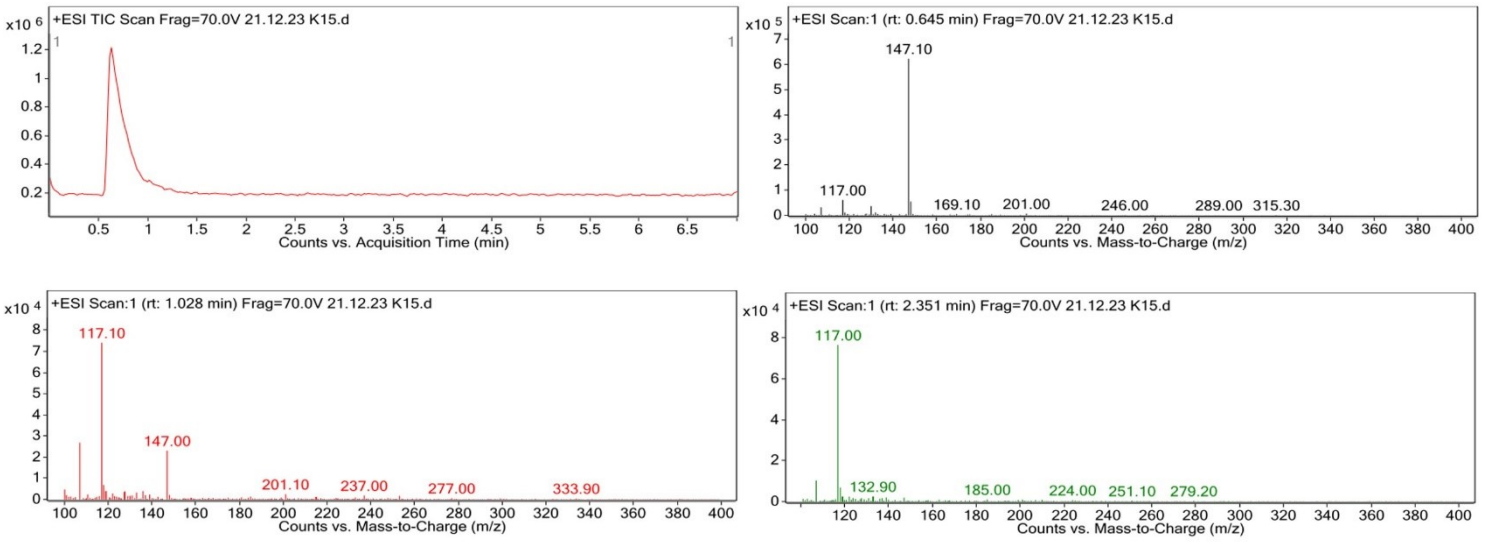

Figure S34. ESI-LC-MS profiles of the catalytic mixture solution by using basic amino acid lysine.

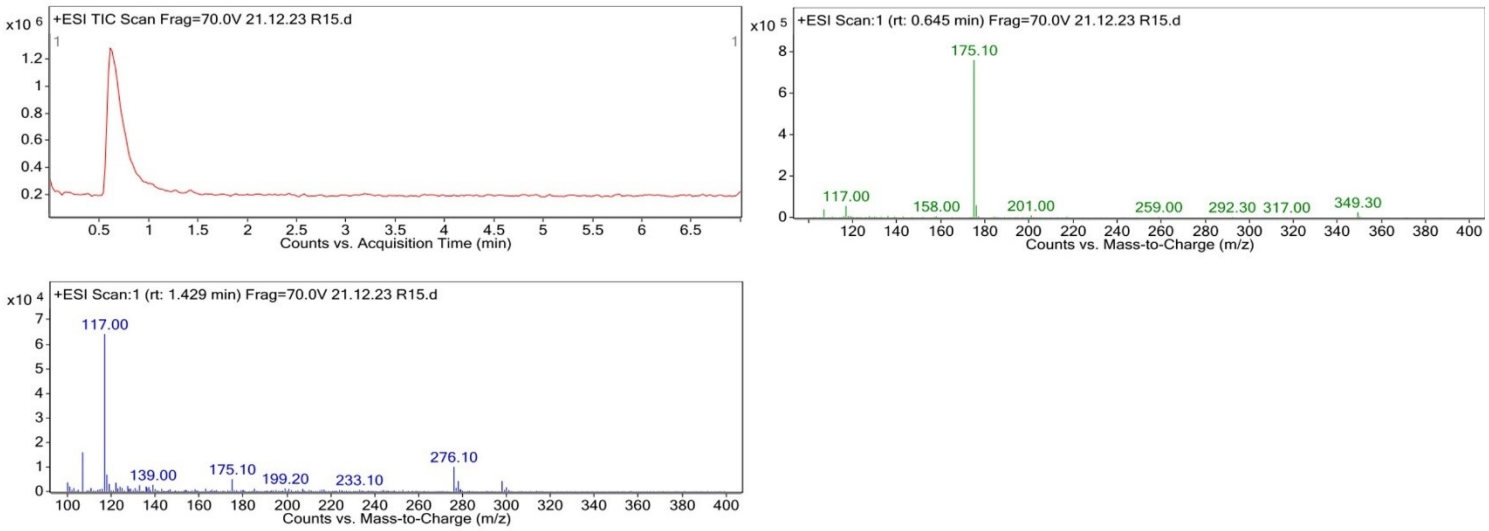

Figure S35. ESI-LC-MS profiles of the catalytic mixture solution by using basic amino acid arginine.

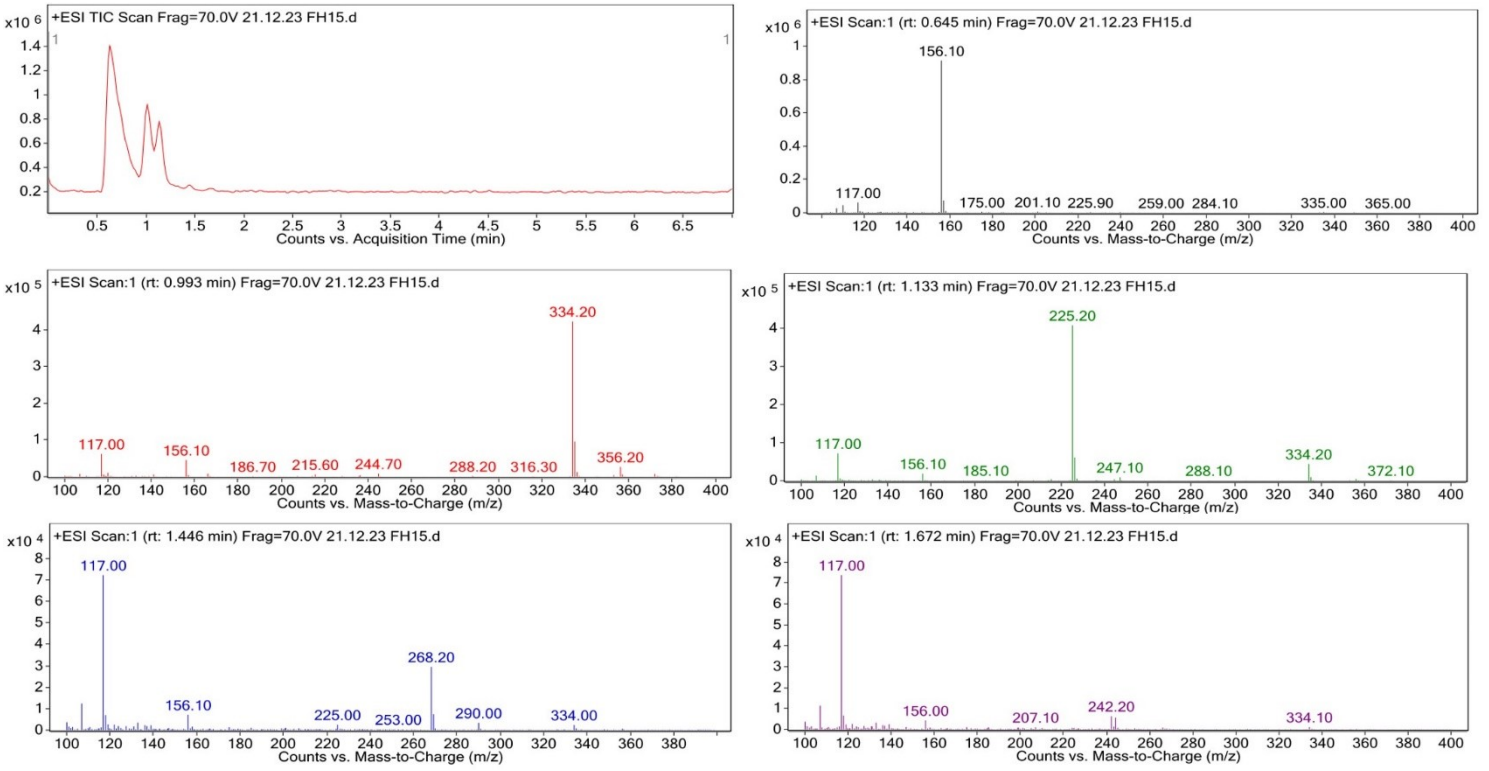

Figure S36. ESI-LC-MS profiles of the catalytic mixture solution by using co-assembled system, **Nap-F$_H$**.

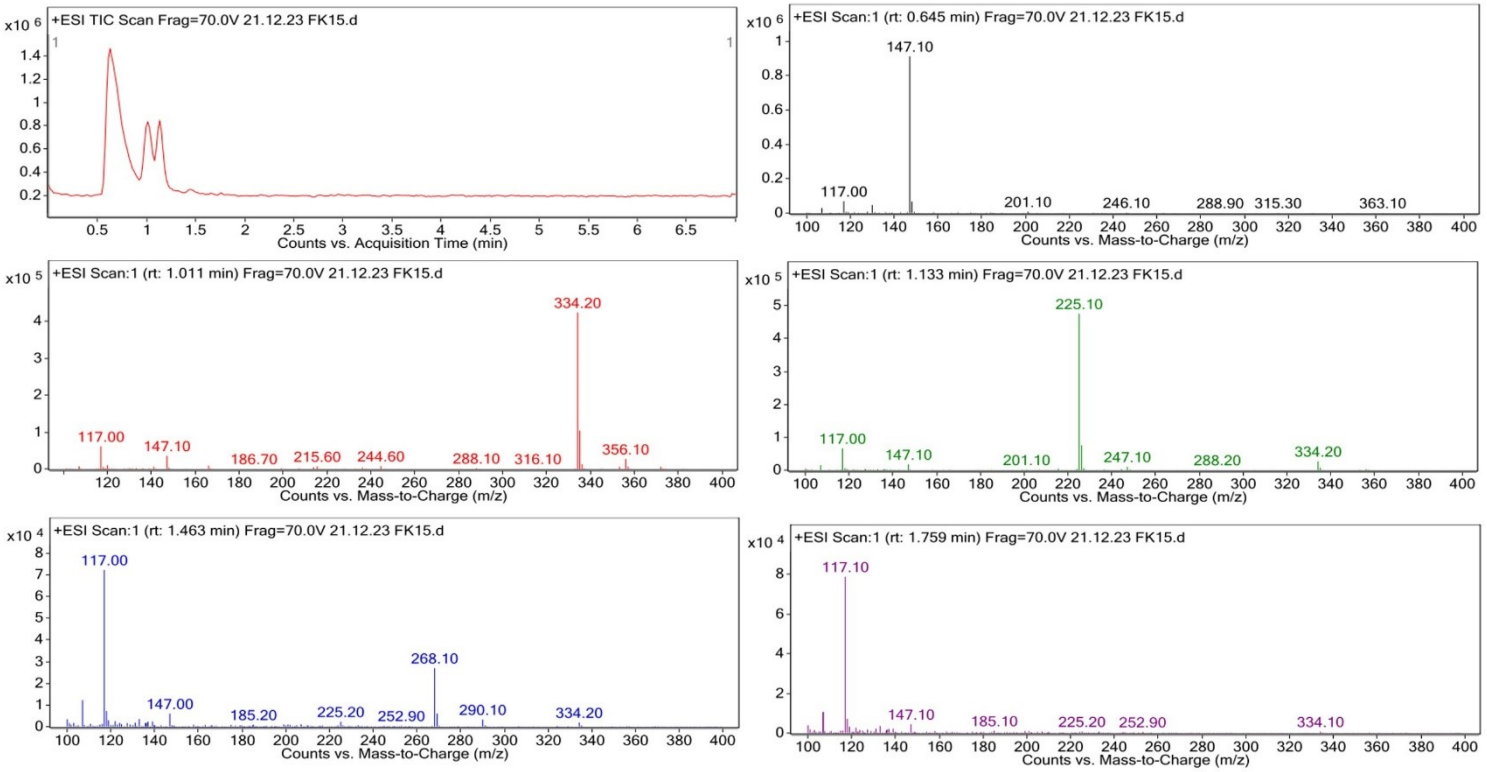

Figure S37. ESI-LC-MS profiles of the catalytic mixture solution by using co-assembled system, **Nap-F$_K$**.

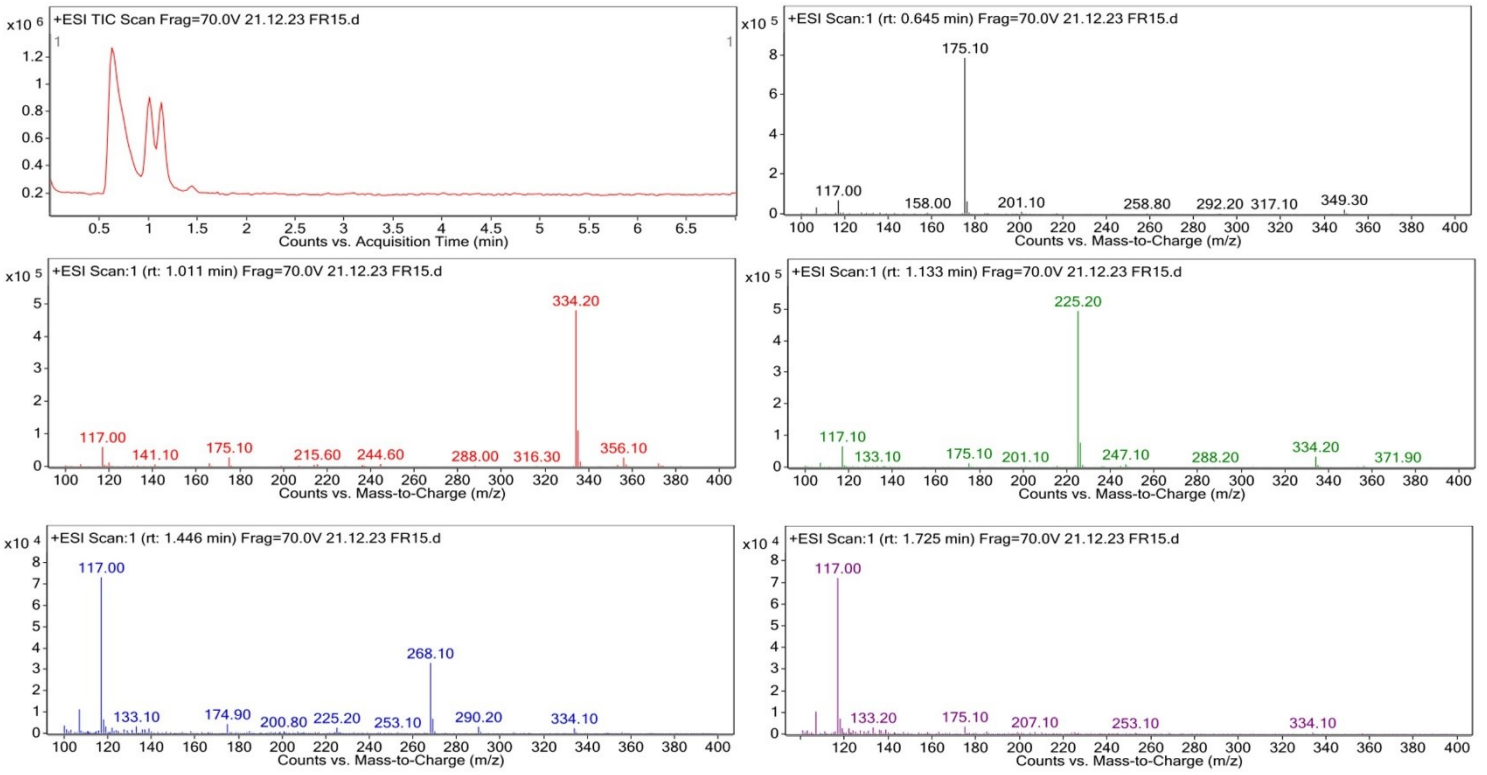

Figure S38. ESI-LC-MS profiles of the catalytic mixture solution by using co-assembled system, **Nap-F$_R$**.

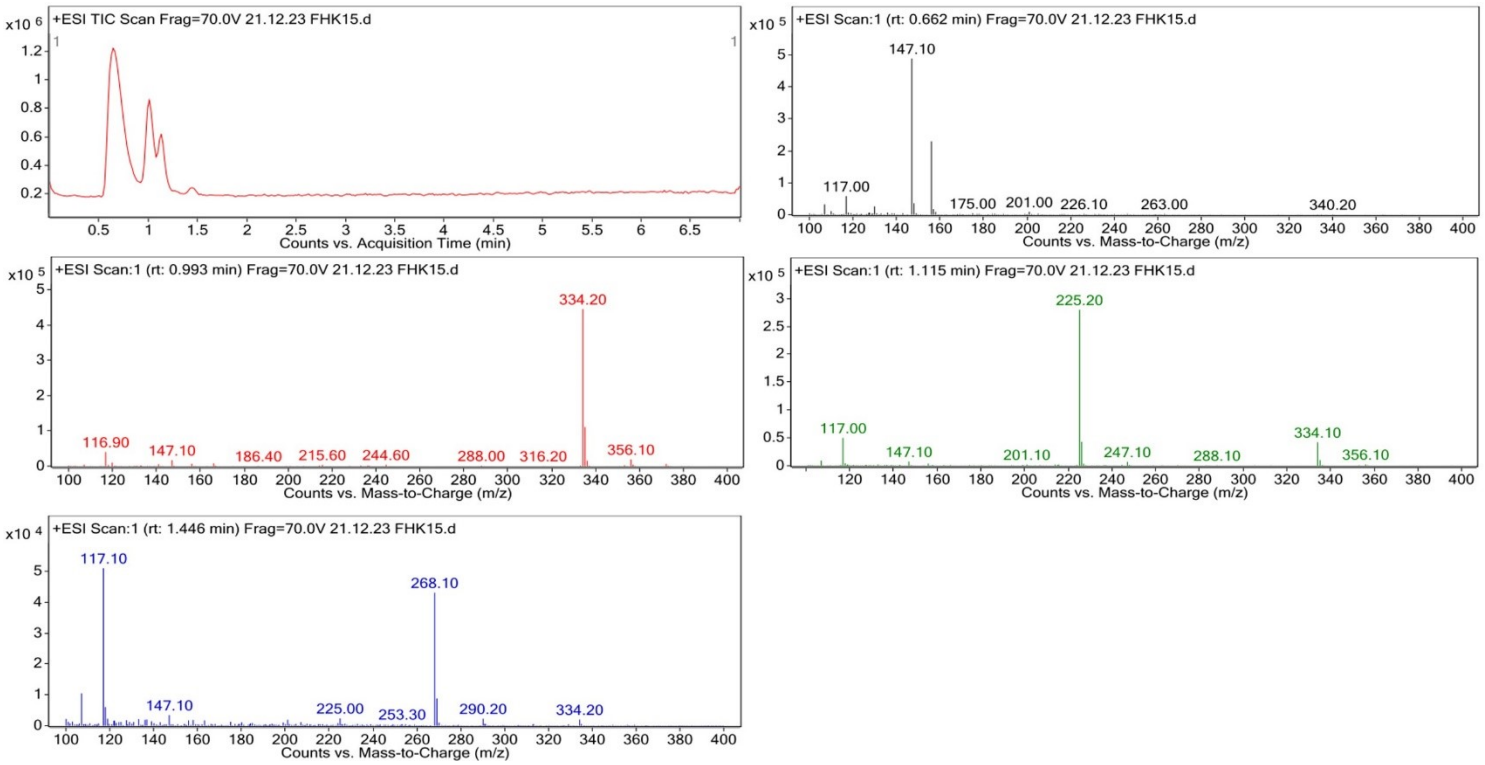

Figure S39. ESI-LC-MS profiles of the catalytic mixture solution by using co-assembled system, **Nap-F$_{H-K}$**.

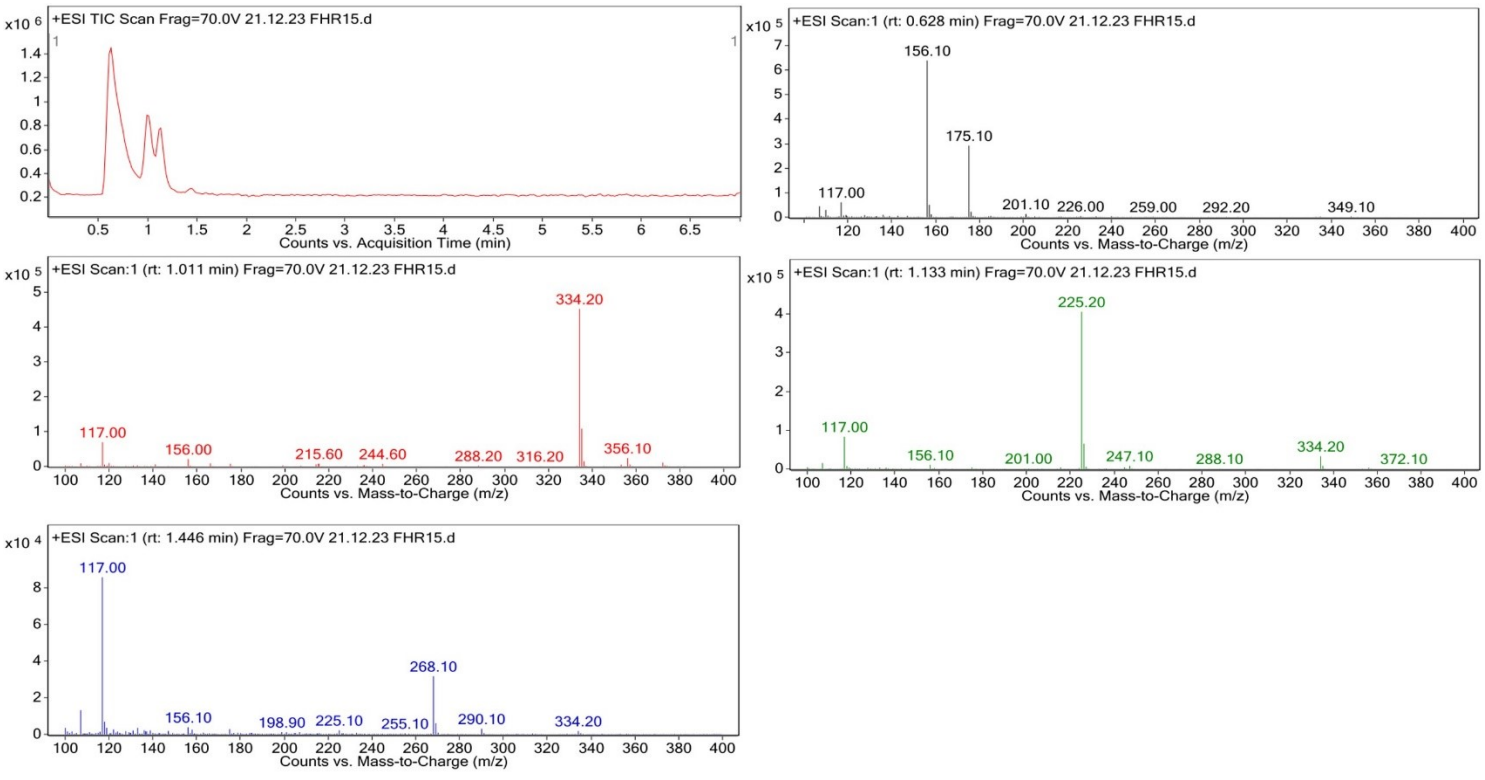

Figure S40. ESI-LC-MS profiles of the catalytic mixture solution by using co-assembled system, **Nap-F$_{H-R}$**.

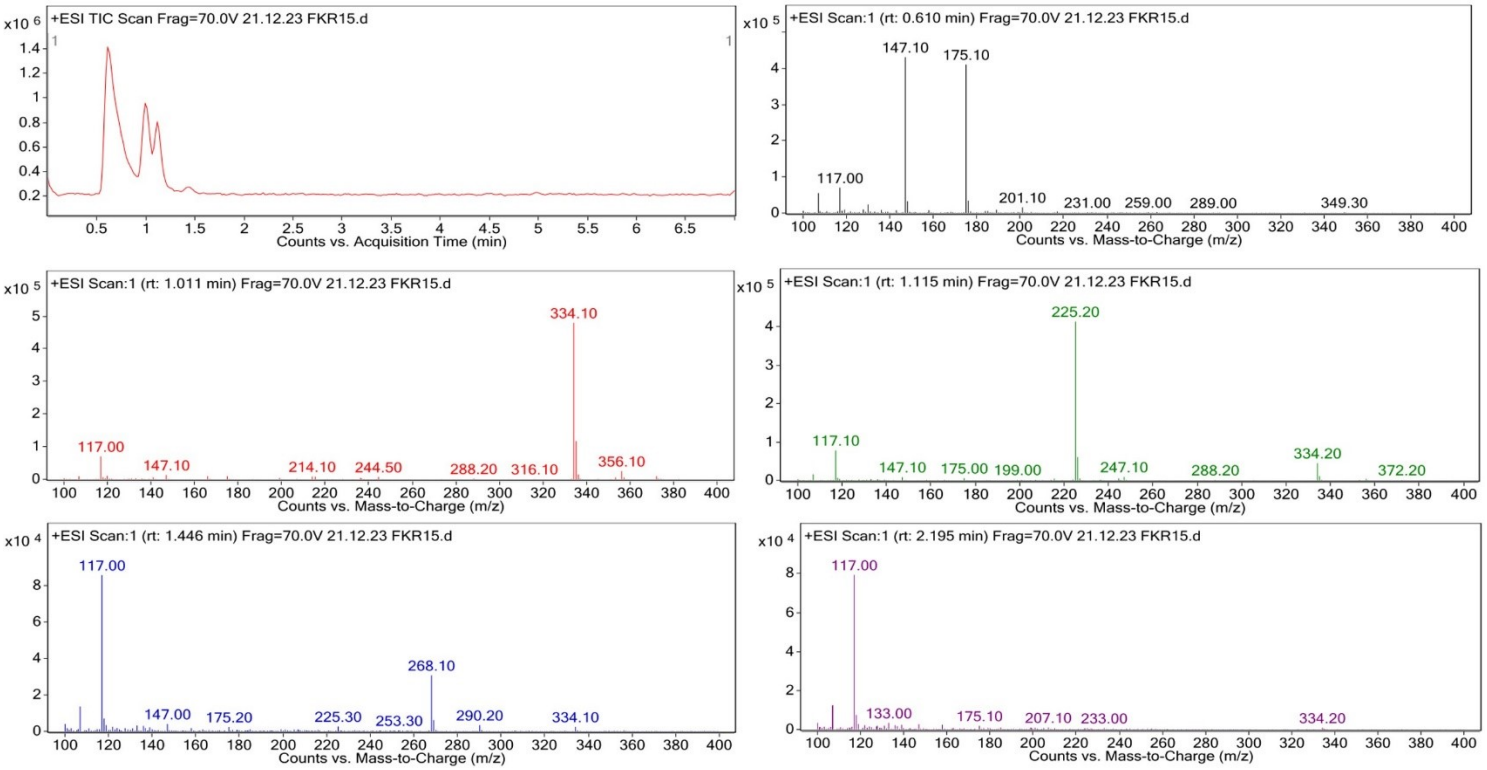

Figure S41. ESI-LC-MS profiles of the catalytic mixture solution by using co-assembled system, **Nap-F$_{K\text{-}R}$**.

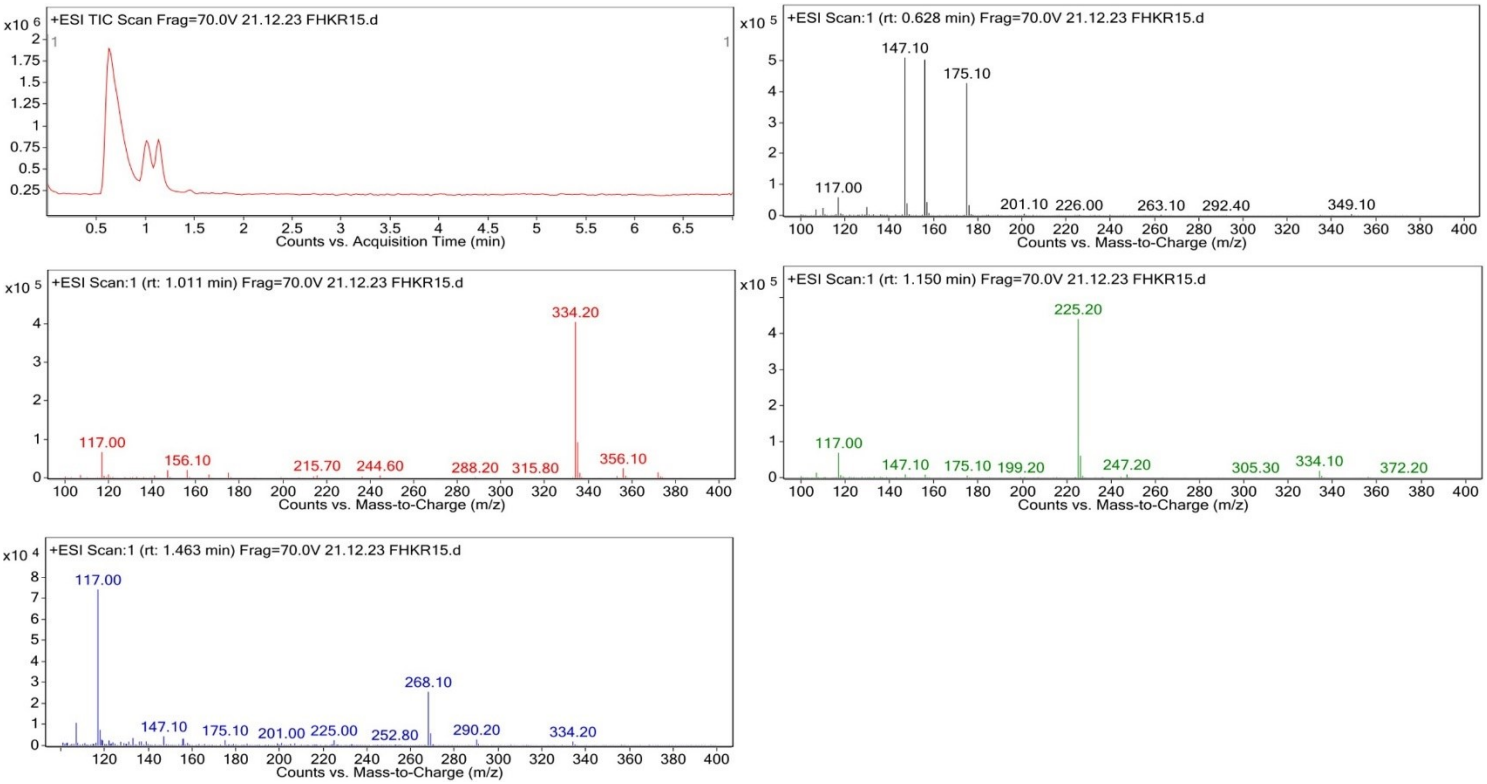

Figure S42. ESI-LC-MS profiles of the catalytic mixture solution by using co-assembled system, **Nap-F$_{H\text{-}K\text{-}R}$**.

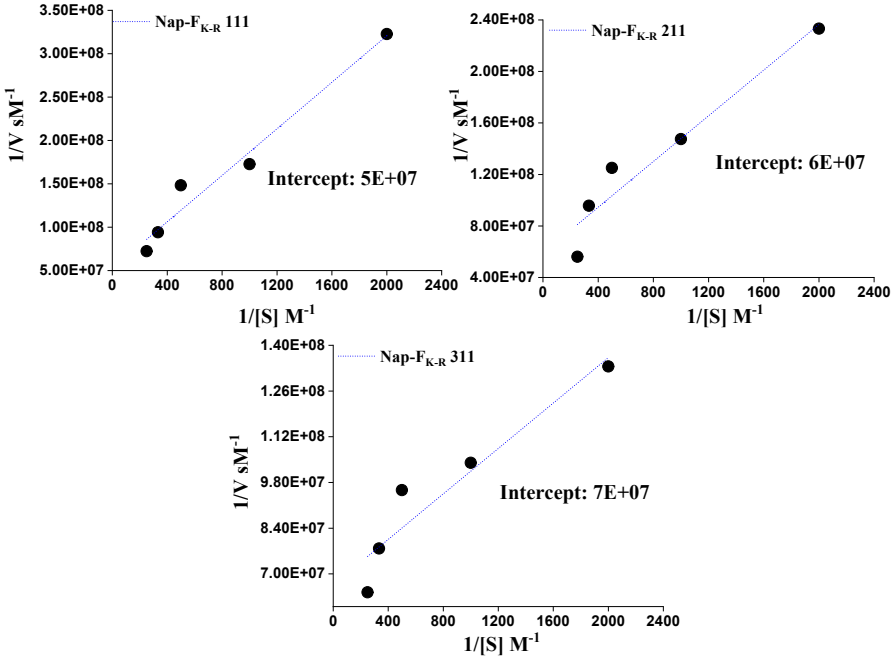

Figure S43. Lineweaver-Bruk plot for the hydrolysis of PNPA using **Nap-F$_{K-R}$** as catalyst keeping the amount of **K** and **R** fixed, the amount of **Nap-F** varied **(a) Nap-F** at 0.1 w/v%, **(b) Nap-F** at 0.2 w/v% and **(d) Nap-F** at 0.3 w/v% for the system 0.3 % w/v, 0.4 % w/v and 0.5 % w/v catalysts respectively.

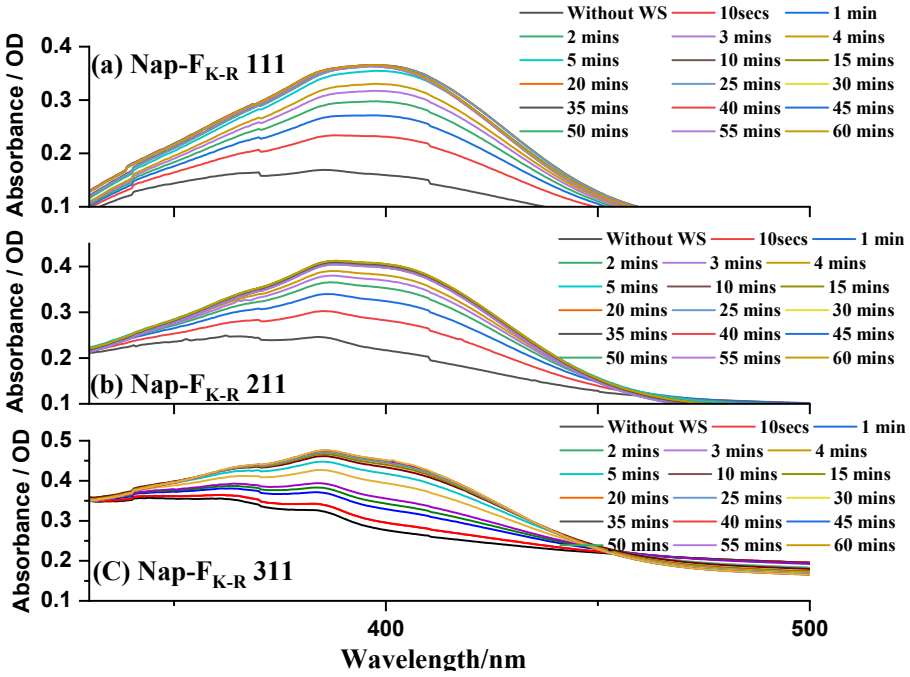

Figure S44. UV-Vis spectra for the hydrolysis of PNPA using **Nap-F$_{K-R}$** as catalyst keeping the amount of **K** and **R** fixed, the amount of **Nap-F** varied **(a) Nap-F** at 0.1 w/v%, **(b) Nap-F** at 0.2 w/v% and **(d) Nap-F** at 0.3 w/v% for the system 0.3 % w/v, 0.4 % w/v and 0.5 % w/v catalysts respectively.

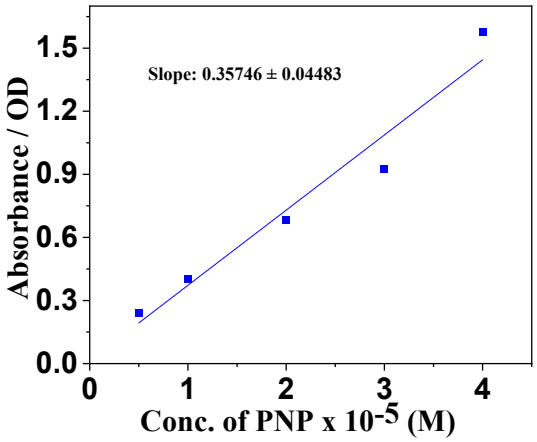

Figure S45. Absorbance vs Concentration plot for determination of molar extinction coefficient (ε) of *p*- nitrophenol at pH 9.00.

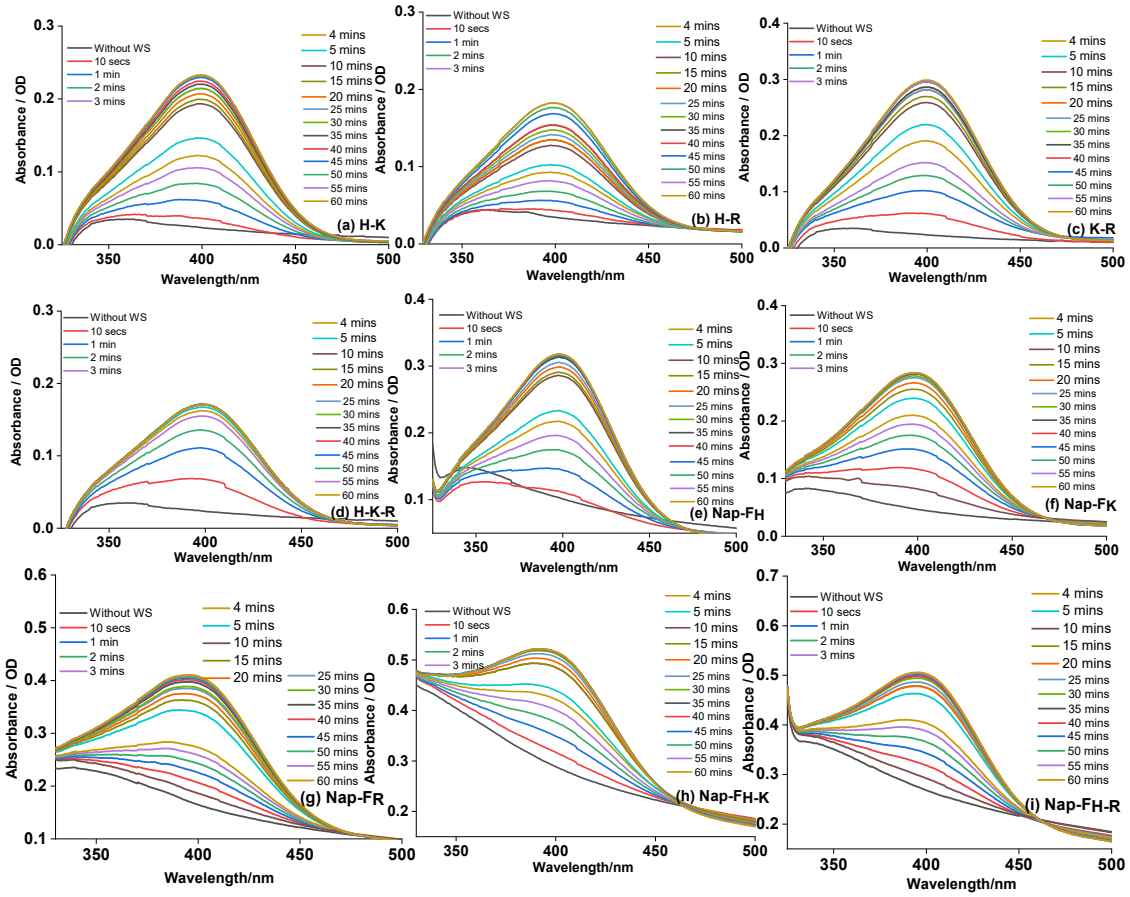

Figure S46. The progress of the *p*-**NPA** to *p*-**NP** hydrolysis reaction monitored at pH 9.00 by time dependent UV-Vis spectroscopic study for the systems including a) **H-K**, (b) **H-R**, (c) **K-R**, (d) **H-K-R**, (e) **Nap-F$_{H}$**, (f) **Nap-F$_{K}$**, (g) **Nap-F$_{R}$**, (h) **Nap-F$_{H-K}$**, (i) **Nap-F$_{H-R}$**, (k) **Nap-F$_{K-R}$**, and (l) **Nap-F$_{H-K-R}$**.

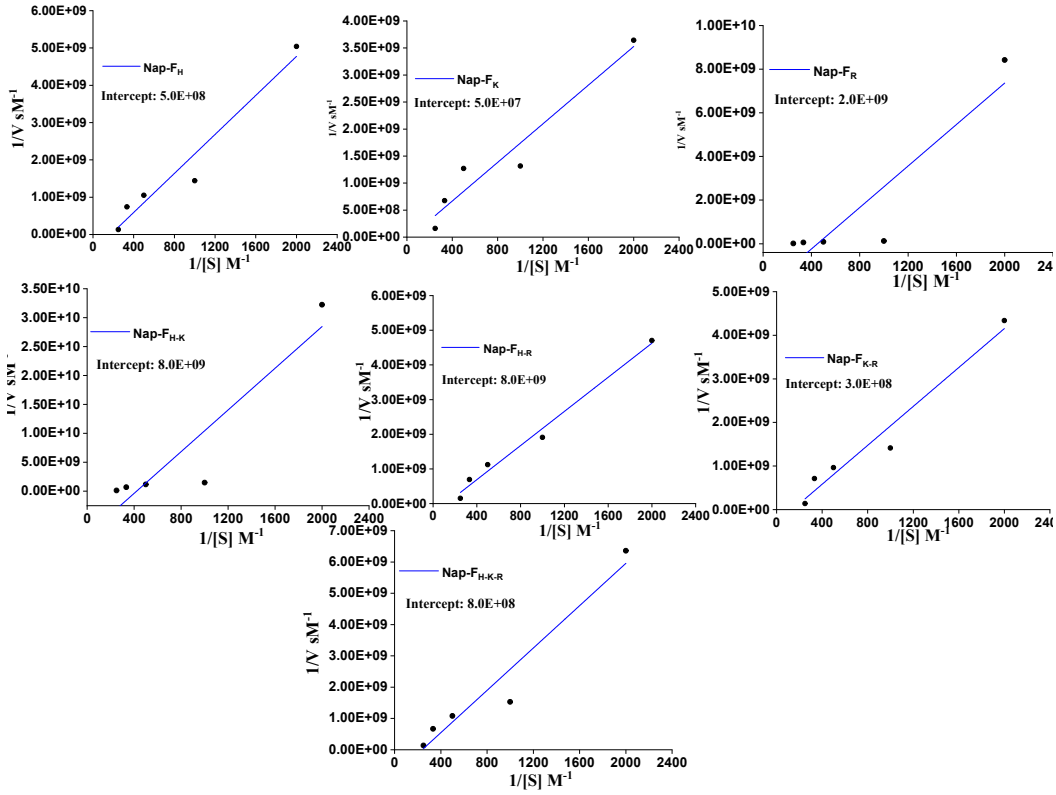

Figure S47. Lineweaver-Bruk plot for the hydrolysis of *p*-**NPA** by using various systems as catalysts at pH 9.00 such as Nap-F_{H}, Nap-F_{K}, Nap-F_{R}, Nap-F_{H-K}, Nap-F_{H-R}, Nap-F_{K-R} and Nap-F_{H-K-R}.

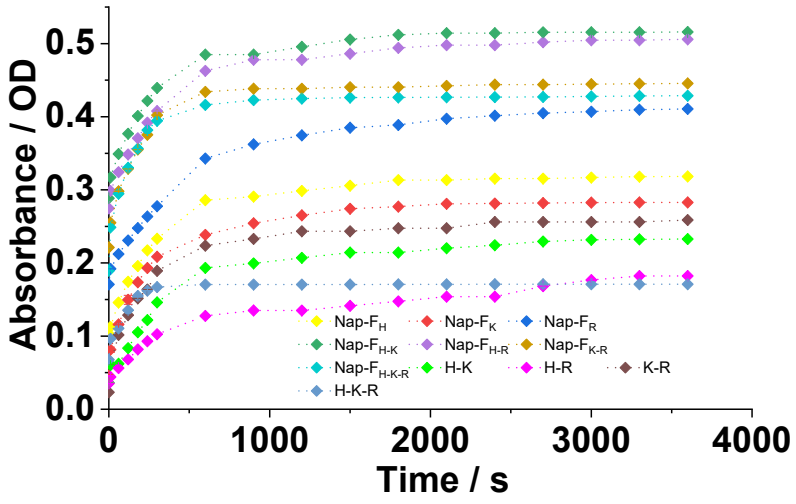

Figure 48. Absorbance versus time spectra for **Nap-F_{H}, Nap-F_{K}, Nap-F_{R}, Nap-F_{H-K}, Nap-F_{H-R}, Nap-F_{K-R}, Nap-F_{H-K-R}, H-R, H-K, K-R and H-K-R** at 0.5% w/v concentrations of pH 9.00 with 3ul working solution of NPA.

Table S6. Kinetic parameters for the hydrolysis of PNPA in the presence of catalyst systems at pH 9.00. The Michaelis–Menten kinetics equation $v = \frac{d[P]}{dt} = \frac{K_{cat}}{K_m}[E]_0[S]$ and double-reciprocal (Lineweaver–Burk) method with the equation $v = \frac{d[P]}{dt} = K_{cat}[E]_0\frac{[S]}{K_M + [S]}$ were used where v is reaction rate, [P] is concentration of product, $[E]_0$ is the initial enzyme concentration, [S] is substrate (p-nitrophenyl acetate) concentration, k_{cat} is the catalytic rate constant, and K_M is the Michaelis constant. The k_{cat}/K_M values calculated from the linear fitting of the double-reciprocal (Lineweaver–Burk) plot (Figure S47).

Catalyst	K_{cat} (s^{-1})	K_M (M)	K_{cat} / K_M (M^{-1} s^{-1})
H-K (2.5:2.5) (0.5% w/v)	2.02×10^{-3}	8.11×10^{-2}	**2.49×10^{-2}**
H-R (2.5:2.5) (0.5% w/v)	1.21×10^{-4}	5.43×10^{-3}	**2.23×10^{-2}**
K-R (2.5:2.5) (0.5% w/v)	1.33×10^{-4}	6.84×10^{-3}	**1.95×10^{-2}**
Nap-F_H (2.5:2.5) (0.5% w/v)	1.635×10^{-4}	6.06×10^{-3}	**2.68×10^{-2}**
Nap-F_K (2.5:2.5) (0.5% w/v)	2.40×10^{-4}	3.63×10^{-2}	**6.61×10^{-2}**
Nap-F_R (2.5:2.5) (0.5% w/v)	1.02×10^{-4}	3.69×10^{-3}	**2.75×10^{-2}**
H-K-R (1.6:1.6:1.6) (0.5% w/v)	3.17×10^{-3}	1.57×10^{-1}	**2.02×10^{-2}**
Nap-F_{H-K} (3:1:1) (0.5% w/v)	1.27×10^{-5}	3.0×10^{-3}	**4.23×10^{-3}**
Nap-F_{H-R} (3:1:1) (0.5% w/v)	3.38×10^{-4}	8.55×10^{-3}	**3.95×10^{-2}**
Nap-F_{K-R} (3:1:1) (0.5% w/v)	3.27×10^{-4}	7.76×10^{-3}	**4.22×10^{-2}**
Nap-F_{R-K-H} (2:1:1:1) (0.5% w/v)	1.62×10^{-4}	4.7×10^{-3}	**3.44×10^{-2}**

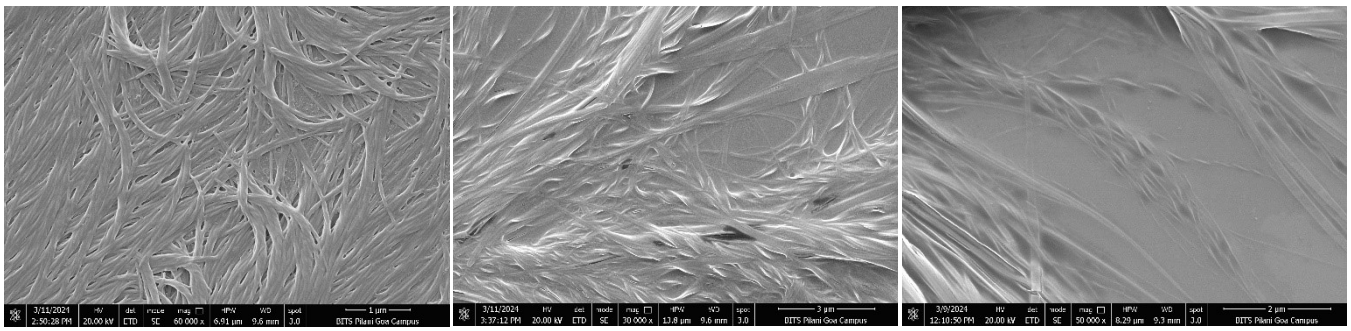

Figure S49. FE-SEM images at assembled solutions of pH 9.00 (50 times dilution for all samples done from 0.5 w/v % co- assembled solution) which have been used for catalytic studies **(a) Nap-F_K** 2.5:2.5, **(b) Nap-F_{H-K}** 3:1:1 and **(c) Nap-F_{K-R}** 3:1:1 (0.5 w/v %).